Cortico-spinal Mechanisms of Periphery Neuromodulation induced Analgesia

Zhaoxing Wei[1,2], Yunyun Duan[3], Yupu Zhu[1,2], Xiaomin Lin[1,2], Ming Zhang[1,2], Jonathan C.W. Brooks[5], Yaou Liu[3*], Li Hu[2,4*], Yazhuo Kong[1,2,6*]

1. CAS Key Laboratory of Behavioral Science, Institute of Psychology, Chinese Academy of Sciences, Beijing 100101, China;
2. Department of Psychology, University of Chinese Academy of Sciences, Beijing 100049, China;
3. Department of Radiology, Beijing Tiantan Hospital, Capital Medical University, Beijing 100070, China;
4. CAS Key Laboratory of Mental Health, Institute of Psychology, Chinese Academy of Sciences, Beijing 100101, China;
5. School of Psychology, University of East Anglia, Norwich, UK;
6. Wellcome Centre for Integrative Neuroimaging, FMRIB, Nuffield Department of Clinical Neurosciences, University of Oxford, Oxford, OX3 9DU, UK

***Corresponding author:** kongyz@psych.ac.cn, huli@psych.ac.cn, liuyaou@bjtth.org

Author contributions

Z.W., L.H., and Y.K. designed the study; Z.W., Y.D., Y.Z., Y.L., and Y.K. performed data acquisition; Z.W., X.L., J.C.W.B., and Y.K. performed data analysis. The original draft was written by Z.W., with Y.K., L.H., M.Z., and J.C.W.B. performing review and editing. All authors reviewed and accepted the final draft of the manuscript.

Potential conflicts of interest

The authors have no conflicts of interest to declare.

Abstract

Nociceptive acute and chronic pain significantly impact the quality of life and create tremendous societal burdens. Given the side effects associated with pharmacological analgesia, noninvasive periphery neuromodulation techniques, like Transcutaneous Electrical Nerve Stimulation (TENS), have emerged as promising approaches for pain relief. Current human research, focusing partly on cerebral, brainstem, or peripheral mechanisms of neuromodulation, lacks comprehensive understanding from the perspective of the entire central nervous system. This study utilized a three-way mixed experimental design, combining cutting-edge cortico-spinal fMRI with thermal stimuli, to systematically explore the central analgesic mechanisms of two typical TENS modes: Conventional (high frequency, low intensity) and Acupuncture-Like (low frequency, high intensity). Behavioral and fMRI analysis revealed that, the direct spinal inhibition (PAG-spinal connectivity) partially mediated by PAG-vmPFC connectivity leads to local analgesic effects in Conventional TENS; a top-down diffuse noxious inhibition (PAG-S1 connectivity) fully mediated through PAG-spinal connectivity leads to diffuse analgesic effects in Acupuncture-Like TENS. Employing advanced cortico-spinal fMRI technique, our findings provide systematic neural evidence of the analgesic mechanisms induced by TENS and shed new light on future neuromodulation approaches.

Keywords: Cortico-spinal fMRI, Pain, Transcutaneous electrical nerve stimulation (TENS), Analgesia

Introduction

Pain is a complex subjective experience with a high prevalence of pathological acute and chronic pain, which affects individuals' quality of life and imposes a societal burden[1,2]. The opioid crisis has brought increased attention to the side effects of pharmacological analgesic methods[3,4]. Nonpharmacological approaches, neuromodulation in particular, are emerging as preferred pain treatments[5]. Non-invasive neuromodulatory techniques, such as Transcutaneous Electrical Nerve Stimulation (TENS) that target the peripheral nervous system, along with Transcranial Magnetic Stimulation (TMS) and Transcranial Direct Current Stimulation (tDCS) that target the central nervous system, primarily the brain, do not necessitate surgical procedures[6].

TENS employs alternating currents with varying frequencies and intensities to stimulate peripheral nerves[7]. Known for being safe, convenient, and low cost[8], TENS has effectively mitigated various pain conditions, e.g., postoperative pain and low back pain[9-12]. TENS generally offers two primary modes: Conventional TENS generates analgesia within targeted dermatomes with higher frequency (~50-100 Hz) and lower intensity (evoking a nonpainful sensation); Acupuncture-Like TENS produces a diffuse analgesic effect that extends beyond the dermatome, with lower frequency (~2-4 Hz) and higher intensity (elicits a tolerable of painful sensation)[13,14].

Previous studies revealed the analgesic effect of non-invasive neuromodulation, but provided limited evidence of the precise neurobiological mechanisms, particularly regarding how they interact with the complex networks of the central nervous system[7,15,16]. Research using animal models has suggested that TENS relieves pain by activating peripheral nerve fibers, thereby modulating (inhibitory or excitatory) pain processing in the central nervous system, along the spinal cord, periaqueductal gray (PAG) of the brainstem, and pain-related cortical regions[17-20]. Specifically, Conventional TENS modifies GABA levels in the dorsal horn and stimulates δ-opioid receptors in the spinal cord and brainstem, while Acupuncture-Like TENS primarily targets local μ-opioid receptors[21,22]. Two theories predominantly explain the efficacy of TENS. Firstly, Conventional TENS is believed to achieve pain relief primarily through spinal inhibition[22-25], in line with the gate control theory and influenced by

supraspinal areas[18,26,27]. Secondly, both TENS modes activate systemic mechanisms, such as the endogenous opioid system or diffuse noxious inhibitory controls (DNIC)[9,28,29], affecting the cortex, brainstem, and notably, the spinal cord.

Recent human studies employing electroencephalography (EEG) and functional magnetic resonance imaging (fMRI) have demonstrated that TENS can modulate spontaneous brainstem activity, particularly in the pons, subnucleus reticularis dorsalis (SRD) and rostral ventromedial medulla (RVM)[14]. Moreover, Conventional TENS has been shown to enhance functional connectivity between the PAG and lateral prefrontal cortex (PFC)[26]. Acupuncture-Like TENS induces more significant changes in alpha oscillations within the primary sensorimotor cortex (S1/M1) and increases the functional connectivity between S1 and the medial PFC more than Conventional TENS[13]. However, human studies directly investigating the entire cortico-brainstem-spinal circuit mechanism in neuromodulation are lacking, leading to a gap in the comprehensive understanding of non-invasive neuromodulation analgesia in human research.

Over the past decade, simultaneous cortico-spinal fMRI has become pivotal in human pain research. This method provides an exceptional opportunity to capture neural activities across the cortex, brainstem, and spinal cord, thus providing systemic insights into the complex neural mechanisms involved in pain processing and neuromodulation[30-32]. Within this framework, the functional networks in the cortico-brainstem-spinal pathway, mainly centering around the PAG, play a multifaceted role in pain modulation[33]. This is evidenced in various contexts, including nocebo hyperalgesia[34], opioid analgesia[35], and attentional analgesia[36]. Consequently, our current study aims to investigate the analgesic mechanisms of both Conventional and Acupuncture-Like TENS, focusing on the comprehensive cortico-brainstem-spinal pathway, especially PAG related endogenous analgesia pathway. Building upon existing literature, we hypothesize that both TENS modes engage the cortico-spinal pain modulation system; their distinct analgesic effects may derive from different neural interactions within this pathway, with the PAG as a relay site but potentially involving direct spinal inhibition or diffuse noxious inhibitory controls.

Results

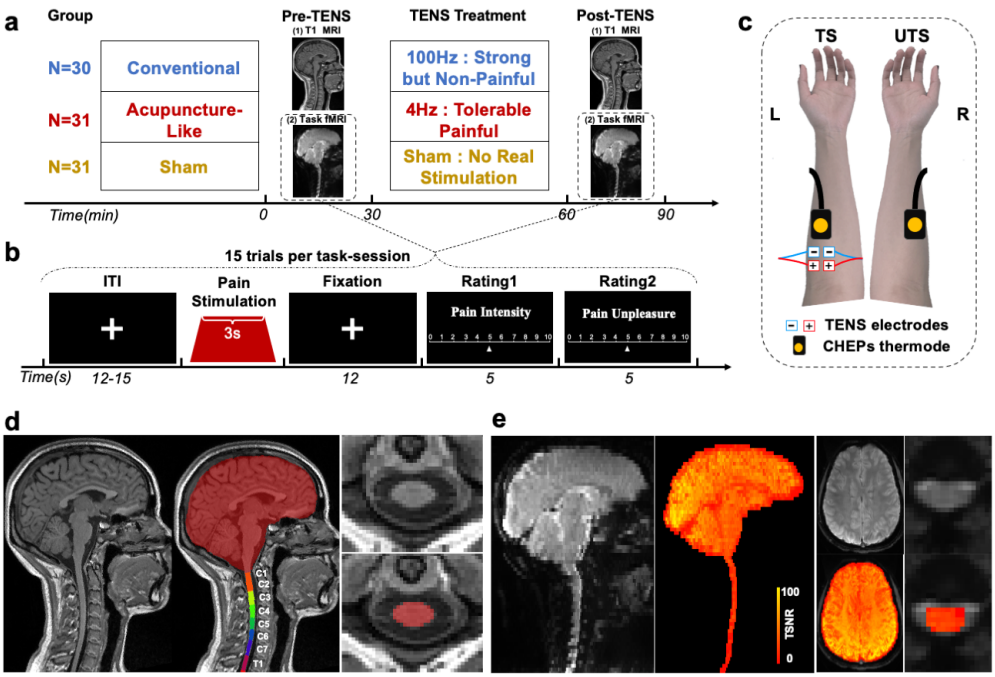

Figure 1. Experimental paradigm. *(**a**) Overview of the experimental process. Participants were assigned to one of three experimental groups to receive different TENS treatments. Cortico-spinal images were acquired before and after TENS treatment. (**b**) Heat pain fMRI paradigm. Heat pain stimulation was applied for 3 seconds, followed by pain intensity and unpleasantness ratings. 15 trials were conducted for each run. (**c**) TENS treatment and heat pain stimulation. TENS electrodes were applied to the C5~C6 dermatome of the left side, while the CHEPS thermode was applied to the same dermatome of both the left and right sides. The left is the treated side (TS), and the right is the untreated side (UTS). (**d**) Bias-corrected T1 images and segment brain and spinal cord examples from one representative participant. (**e**) Data quality check: distortion and physiological noise corrected fMRI image and corresponding temporal signal-to-noise ratio (tSNR) map of segmented cortico-spinal areas (sagittal and transversal views) from one representative participant.*

Participants were randomly assigned to one of three distinct groups: Conventional TENS (*N*=30), Acupuncture-Like TENS (*N*=31), and sham TENS (*N*=31), each receiving a specific TENS treatment. Specifically, our experiment adopted a three-way mixed design with a 3 (group: Conventional, Acupuncture-Like, sham) × 2 (side: left treated side, TS; right untreated side, UTS) × 2 (order: pre-TENS, post-TENS)

128 paradigm (**Fig. 1a-c).** TENS was applied to the C5~C6 dermatome based on Natter's
129 Atlas of Human Neuroscience[37] of the left forearm (treated side, TS). Heat pain
130 stimulation was applied to the same dermatome on both the left (treated) and right
131 (untreated) sides, and the order was pseudorandomized across participants.
132 Simultaneous cortico-spinal scans of structural and task-based functional MRI with
133 heat stimuli were obtained before and after TENS treatment. One-way analysis of
134 variance (ANOVA) revealed no significant differences among the three groups in
135 demographic variables, pain cognition, and emotion (**Supplementary Table 1**), as well
136 as Quantitative Sensory Test (QST) indices **(Supplementary Table 2).**

137 ***Psychophysics of pain intensity and unpleasantness with TENS modulations***

138 Experimental pain is characterized by two dimensions: sensory discrimination,
139 reflected as pain intensity[38], and affective-motivational, manifested as unpleasantness[39].
140 Accordingly, we collected pain intensity and unpleasantness ratings for each stimulus
141 during the pre and post-TENS heat pain fMRI sessions. A 3 "group" × 2 "side" × 2
142 "order" mixed-design ANOVA revealed significant interaction effects for pain
143 intensity ($F_{(2,89)} = 28.80$, $P < 0.001$) and unpleasantness ($F_{(2,89)} = 14.50$, $P < 0.001$),
144 indicating different analgesic effects across the three TENS groups.

145 To further dissect the analgesic effects, we implemented a 2 (side: TS, UTS) × 2 (order:
146 pre-TENS, post-TENS) repeated-measures ANOVA within each TENS treatment
147 group **(Fig. 2a, d).** In the Conventional TENS group, significant "side" × "order"
148 interaction effects emerged for pain intensity ($F_{(1,29)} = 38.60$, $P < 0.001$) and
149 unpleasantness ($F_{(1,29)} = 20.70$, $P < 0.001$). Post hoc paired t-tests revealed a significant
150 analgesic effect in TS (pain intensity: $t_{(29)} = 6.87$, $P < 0.001$, unpleasantness: $t_{(29)} = 5.25$,
151 $P < 0.001$) but not in UTS, suggesting a localized analgesic effect of Conventional
152 TENS within the treated dermatome. In the Acupuncture-Like TENS group, we
153 observed significant main effects for "order" (pain intensity: $F_{(1,30)} = 37.94$, $P < 0.001$;
154 unpleasantness: $F_{(1,30)} = 19.13$, $P < 0.001$) and "side" (pain intensity: $F_{(1,30)} = 21.50$, $P <$
155 0.001; unpleasantness: $F_{(1,30)} = 11.17$, $P = 0.002$), but no significant interaction effect.
156 Post hoc paired t-test found a significant analgesic effect in both the TS (pain intensity:
157 $t_{(30)} = 5.47$, $P < 0.001$; unpleasantness: $t_{(30)} = 4.47$, $P < 0.001$) and UTS (pain intensity:
158 $t_{(30)} = 6.04$, $P < 0.001$; unpleasantness: $t_{(30)} = 3.75$, $P < 0.001$), indicating diffuse

analgesic effects even for untreated dermatome from Acupuncture-Like TENS. The sham TENS group had no significant analgesic effect in either TS or UTS.

To directly quantify and compare the analgesic effects (Δpain intensity and Δunpleasantness, pre-TENS minus post-TENS) across groups, we conducted a 3 (group: Conventional, Acupuncture-Like, Sham) × 2 (side: TS, UTS) mixed-design ANOVA **(Fig. 2b, e)**. We detected a significant interaction effect between "group" and "side" in Δpain intensity ($F_{(2,89)} = 27.10$, $P < 0.001$) and Δunpleasantness ($F_{(2,89)} = 14.50$, $P < 0.001$), suggesting different analgesic effects among the three TENS modes. The Conventional TENS group exhibited significant differences between TS and UTS in terms of Δpain intensity($t_{(89)} = -8.79$, $P < 0.001$) and Δunpleasantness ($t_{(89)} = -6.64$, $P < 0.001$). However, no differences were observed between TS and UTS in the Acupuncture-Like and sham TENS groups.

Additionally, we employed Pearson correlation analysis to investigate the relationship between TS and UTS analgesic effects within each group **(Fig. 2c, f)**. A significant positive correlation between TS and UTS analgesic effects (Δpain intensity: $r = 0.73$, $P < 0.001$; Δunpleasantness: $r = 0.76$, $P < 0.001$) was observed exclusively in the Acupuncture-Like TENS group, i.e. regardless of the treatment location, both sides showed consistent analgesic pattern. No such correlation was detected in the Conventional TENS or sham TENS group.

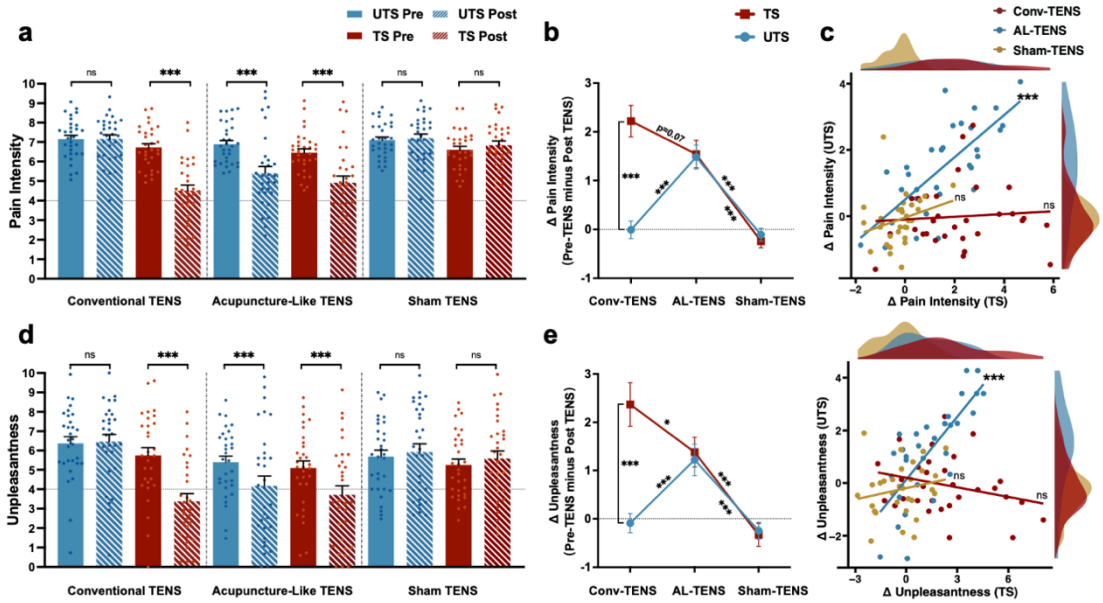

Figure 2. Behavioral ratings. *(**a, d**) Pain intensity and unpleasantness rating results of the three groups. In the Conventional TENS group, pain perception was significantly reduced after treatment only in TS. In the Acupuncture-Like TENS group, both the TS and UTS demonstrated significant reductions in pain perception. However, neither side showed significant pain modulation in the sham TENS group. (**b, e**) Analgesic effect (pre minus post) of pain intensity and unpleasantness showed the strongest effect in the TS of the Conventional TENS group. (**c, f**) Correlations of the analgesic effects (Δpain intensity and Δunpleasantness) between TS and UTS in each group revealed a significant positive correlation only for the Acupuncture-Like TENS group. Dots represent the individual participant values, and error bars indicate the SEM. * P < 0.05; ** P < 0.01;*** P < 0.001; ns: not significant.*

Brain and spinal cord blood-oxygen-level-dependent (BOLD) activations

Group average BOLD activations from the cervical cord to the cortex, induced by heat pain stimulation prior to TENS treatment, were observed in classical pain-associated regions **(Supplementary Fig. 2)**. These included primary and secondary somatosensory cortices (S1 and S2), primary motor cortex (M1), supplementary motor area (SMA), anterior cingulate cortex (ACC), insula, thalamus, cerebellum, PAG, RVM (cluster-forming threshold Z > 3.1, family-wise error (FWE) corrected P < 0.05), and the dorsal areas of C6 segments of the spinal cord (P < 0.05, threshold-free cluster enhancement (TFCE) corrected).

To investigate TENS-induced modulation of activities across the entire cortico-spinal pathway, we implemented a group-level General Linear Model (GLM) model of 2 (side: TS, UTS) × 2 (order: pre-TENS, post-TENS) repeated-measures ANOVA on the simultaneous cortico-spinal fMRI data for each group. Please note that to control the lateralization bias between left- and right-side nociceptive stimulation[40,41] we flipped the X dimension of each subject's right-side heat pain-activated first-level parameter estimation images for higher-level group comparisons. Whole brain analysis after multiple comparisons indicated that Conventional TENS exerted a localized modulatory effect (interaction) on heat pain-evoked activation in the TS but not in UTS at the cortico-spinal level **(Fig. 3)**. Conversely, Acupuncture-Like TENS demonstrated a diffuse modulatory effect (main effect of "order") on heat pain-evoked activation in both the TS and UTS **(Fig. 4)**.

Specifically, within the Conventional TENS group, a significant interaction contrast showed several pain-associated regions along the cortico-spinal pathway **(Fig. 3)**, including cortical areas of the left S2 (cluster forming threshold $Z > 3.1$, FWE corrected $P < 0.05$), ventromedial PFC (vmPFC), PAG, RVM as well as spinal cord C6 segments (TFCE corrected, $P < 0.05$). Parameter estimates (PEs) were extracted from the regions showing significant interaction effects for post-hoc t-tests. In particular, the S2 ($t_{(29)} = 4.03$, $P < 0.001$), PAG ($t_{(29)} = 4.78$, $P < 0.001$), RVM ($t_{(29)} = 3.73$, $P < 0.001$), and spinal cord ($t_{(29)} = 4.59$, $P < 0.001$) demonstrated significant decreases in heat pain activation, while the vmPFC exhibited a significant increase in activation ($t_{(29)} = -3.33$, $P = 0.002$) in TS. In the UTS, we detected a non-significant modulation in activation in the S2 and PAG, while significant activation increases were observed in RVM ($t_{(29)} = -2.61$, $P = 0.01$) and spinal cord ($t_{(29)} = -2.23$, $P = 0.03$). No significant decrease in vmPFC activation ($t_{(29)} = 1.41$, $P = 0.17$) was found in response to heat pain stimulation in the UTS **(Fig. 3b-f).**

We did not identify regions with significant interaction effects within the Acupuncture-Like TENS group. However, we observed the significant main effect of "order" in several regions, including the right SMA, dorsal ACC (dACC), bilateral S1, S2, left cerebellum (cluster-forming threshold $Z > 3.1$, FWE corrected $P < 0.05$), PAG, as well as spinal cord C6 segment ($P < 0.05$, TFCE corrected, **Fig. 4)**. Parameter estimates were extracted for post-hoc t-tests from regions with a significant main effect of "order".

ROI analysis indicated significant activity decreases in both TS and UTS within the S1, SMA, dACC cluster (TS: $t_{(30)} = 3.64$, $P = 0.001$; UTS: $t_{(30)} = 2.93$, $P = 0.006$), bilateral S2 (TS: $t_{(30)} = 5.42$, $P < 0.001$; UTS: $t_{(30)} = 4.62$, $P < 0.001$), PAG (TS: $t_{(30)} = 2.70$, $P = 0.01$; UTS: $t_{(30)} = 2.01$, $P = 0.05$) and spinal cord (TS: $t_{(30)} = 2.40$, $P = 0.02$; UTS: $t_{(30)} = 3.62$, $P = 0.001$). Unlike the Conventional TENS group, the vmPFC did not show a significant change of activities in either TS ($t_{(30)} = -1.53$, $P = 0.14$) or UTS ($t_{(30)} = -1.43$, $P = 0.16$) **(Fig. 4b-f)**.

The sham TENS group did not exhibit either significant main effect of "order" or interaction effect. Other detailed brain ANOVA results for each group are provided in **Supplementary Figure 3.**

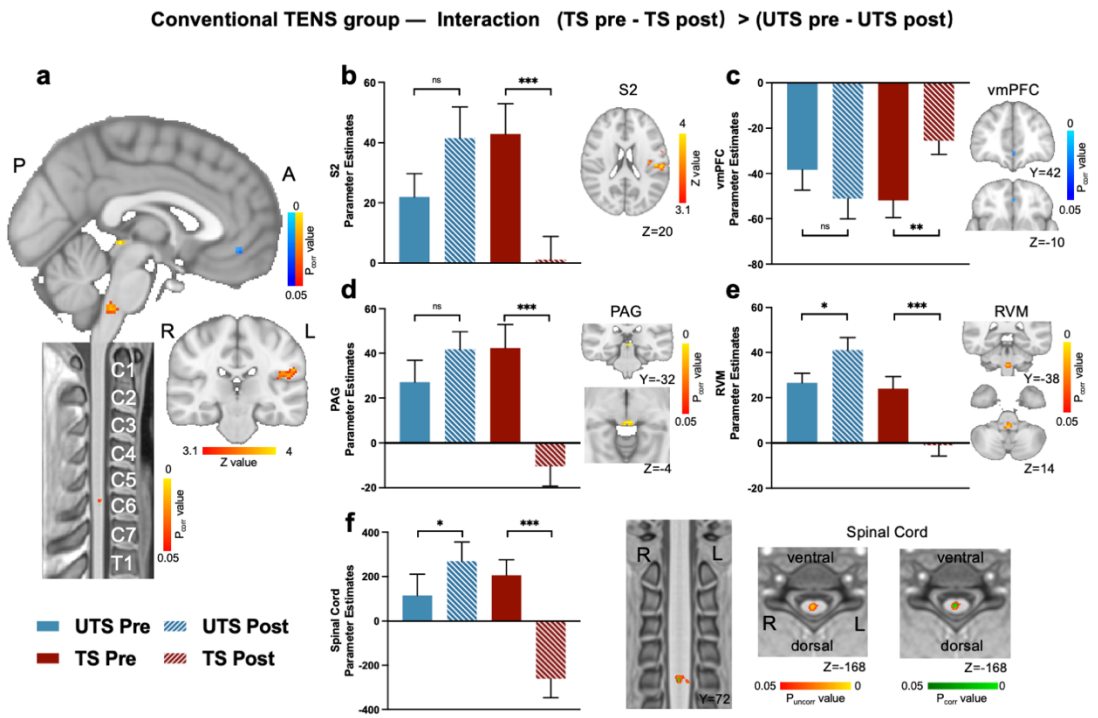

Figure 3. Modulations of BOLD responses in the brain and spinal cord due to Conventional TENS. *(a) The Conventional TENS group showed a significant interaction effect in the left S2 (cluster forming threshold Z > 3.1, FWE corrected P < 0.05), vmPFC, PAG, RVM, and spinal cord C6 segment (P < 0.05, TFCE corrected); (**b**) Parameter estimates (PE) of ipsilateral S2 showed a significant decrease for TS after TENS treatment; (**c**) PEs of vmPFC showed a significant increase for TS after TENS treatment; (**d**) PEs of dorsal lateral PAG showed a significant decrease of TS*

*after TENS treatment; (**e**) PEs of RVM showed a significant decrease for TS and an increase for UTS after TENS treatment; (**f**) The first panel: PEs of the C6 spinal cord showed a significant decrease for TS after TENS treatment; the second panel: coronal view of statistical z-maps overlaid on a PAM50 T1 image; the third panel: axial view with the threshold set to $P_{uncorr} < 0.05$ for visualization (red); the fourth panel: axial view with the threshold set to $P_{corr} < 0.05$. * $P < 0.05$; ** $P < 0.01$;*** $P < 0.001$; ns: not significant.*

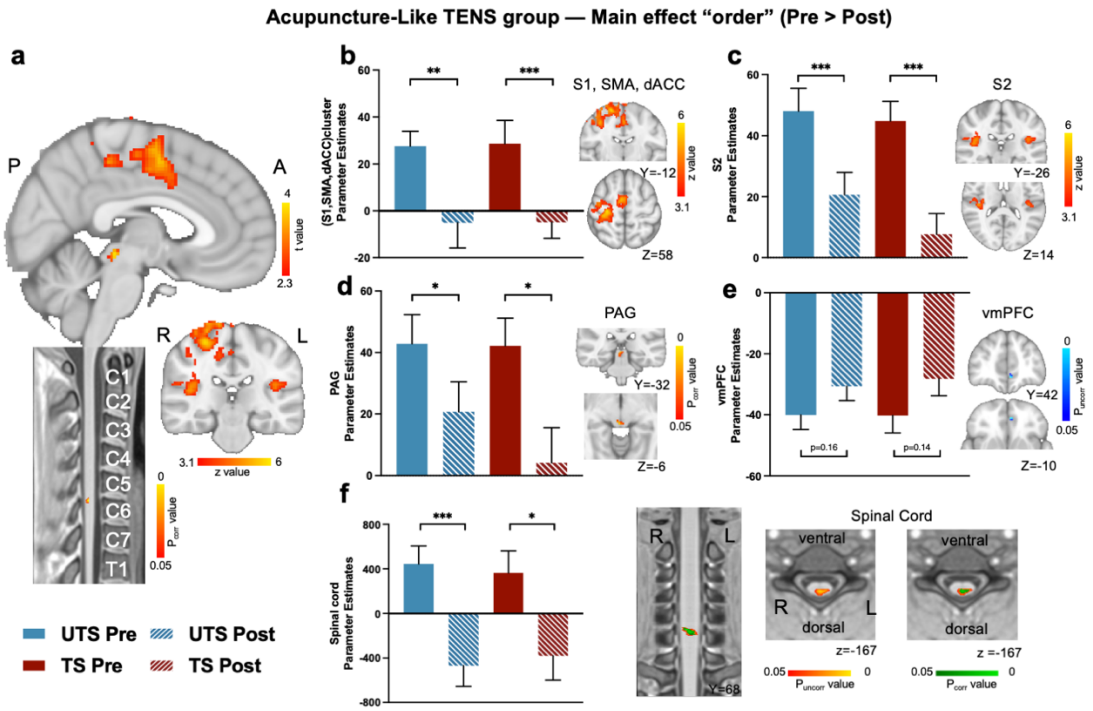

Figure 4. Modulation of BOLD responses in the brain and spinal cord due to Acupuncture-Like TENS. *(**a**) The Acupuncture-Like TENS group showed a significant main effect of "order" in the S1, S2, dACC, SMA (cluster forming threshold $Z > 3.1$, FWE corrected $P < 0.05$), PAG, and spinal cord C6 segment ($P < 0.05$, TFCE corrected); (**b**) PEs of right S1, dACC, SMA cluster showed decreases in both TS and UTS after TENS treatment; (**c**) PEs of bilateral S2 showed decreases in both TS and UTS after TENS treatment; (**d**) PEs of ventral lateral PAG showed decreases in both TS and UTS after TENS treatment; (**e**) PEs of vmPFC showed non-significant increases in both TS and UTS after TENS treatment; (**f**) The first panel: PEs of the spinal cord showed decreases in both TS and UTS after TENS treatment; the second panel: coronal view of statistical z-maps overlaid on a PAM50 T1 image; the third panel: axial view*

*with the threshold set to $P_{uncorr} < 0.05$ for visualization (red – yellow); the fourth panel: axial view with the threshold set to $P_{corr} < 0.05$ (green). * $P < 0.05$; ** $P < 0.01$;*** $P < 0.001$.*

PAG activity associated with local and diffuse analgesic effects of TENS

Our study specifically focused on the PAG, a core region involved in pain perception and the descending modulation of pain signals. We examined the relationship between ΔPAG activity (pre-TENS minus post-TENS) and the analgesic effects (Δpain intensity, also pre-TENS minus post-TENS) in both TENS groups. In the Conventional TENS group, ΔPAG activity significantly positively correlated with the Δpain intensity (R^2 = 0.45, β = 0.01, SE = 0.00, t = 2.55, P = 0.01), and the difference in effects between the TS and the UTS was statistically significant (β = -1.71, SE = 0.41, t = -4.20, P < 0.001). Further correlation analysis revealed a significant positive correlation between Δpain intensity and ΔPAG activity in the TS (r = 0.39, P = 0.04) but not in the UTS (r = 0.22, P = 0.23) **(Fig. 5a, c)**. In the Acupuncture-Like TENS group, ΔPAG activity significantly positively correlated with the Δpain intensity (R^2 = 0.18, β = 0.01, SE = 0.00, t = 3.60, P < 0.001). However, the effect difference between the TS and the UTS was insignificant (β = 0.08, SE = 0.00, t = 3.60, P = 0.81) **(Fig. 5b, d)**.

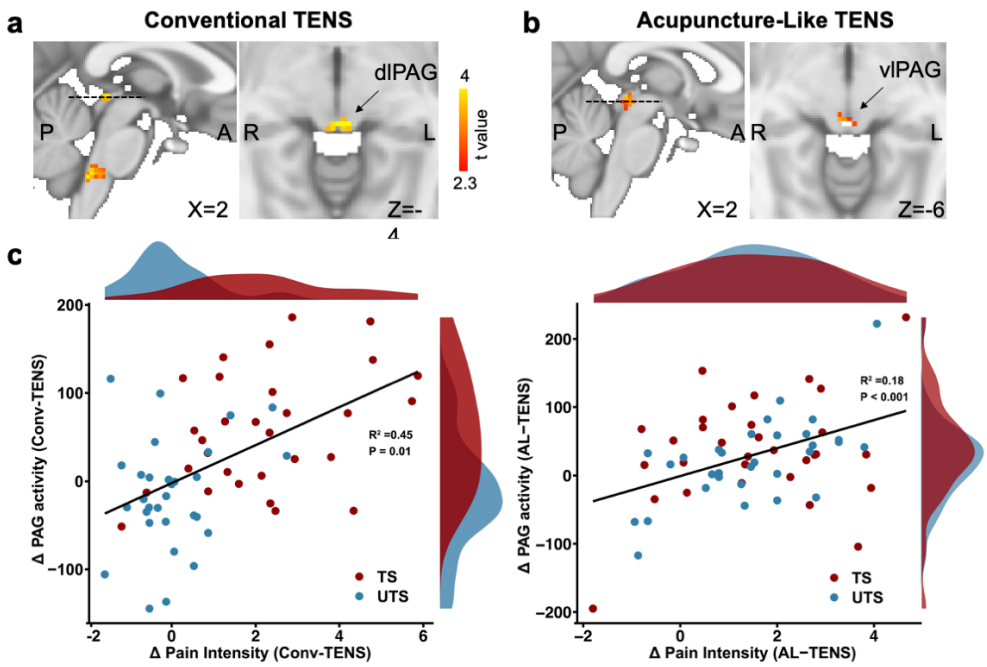

Figure 5. PAG activity correlated with the analgesic effect of TENS. *(**a**) Left dlPAG (ipsilateral TENS treatment) significantly decreased TS activation in the Conventional TENS group. (**b**) Right vlPAG (contralateral TENS treatment) showed the main "order" effect in the Acupuncture-Like TENS group, in which both the TS and UTS showed a significant decrease in activation. (**c**) Conventional TENS group: Δdorsal lateral PAG (dlPAG) activity has a significant positive correlation with the Δpain intensity (R^2 = 0.45, β = 0.01, P = 0.01), and the difference in effects between the TS and the UTS was statistically significant (β = -1.71, P < 0.001). (**d**) Acupuncture-like TENS group: Δventral lateral PAG (vlPAG) activity has a significant positive correlation with the Δpain intensity (R^2 = 0.18, β = 0.01, P < 0.001). However, the effect difference between the TS and the UTS was insignificant (β = 0.08, P = 0.81).*

PAG-based cortical-spinal TENS analgesic pathways

To delve deeper into the cooperation between brain and spinal cord regions under different neuromodulation conditions along the entire cortico-spinal pathways, psycho-physiological interaction (PPI) analyses were employed. For the first-level PPI analysis, the PAG served as a seed region to explore its coupling with areas identified from ANOVA results and previous literature[13,26,42], including bilateral S1, vmPFC, and C5-C7 cervical cord. A 2 × 2 within-group repeated-measures ANOVA was performed for

the group-level PPI analysis. Subsequently, mediation analysis with 1000 bootstraps was applied to integrate significant PPI changes (Δconnectivity, pre-TENS minus post-TENS) with behavioral analgesic effects to uncover the potential mechanisms behind TENS-induced analgesia. We find different contributions of PAG-spinal and PAG-cortical connectivities in mediating the analgesic effects elicited by the two modes of TENS.

In the Conventional TENS group (**Fig. 6a)**, a significant interaction effect was noted for PAG-vmPFC connectivity (left vmPFC, ipsilateral to TENS stimulus, $P < 0.05$, TFCE corrected), primarily dominated by a significant increase in TS ($t_{(29)} = -2.10$, $P = 0.04$) and a non-significant decrease in UTS**.** For PAG-spinal connectivity, a significant interaction effect ($P < 0.05$, TFCE corrected) was also found due to a significant decrease in TS ($t_{(29)} = 4.92$, $P < 0.001$) and a non-significant increase in UTS**.** Furthermore, the change in PAG-spinal connectivity (ΔPAG-spinal) was found to have a significant positive correlation with the Δpain intensity ($r = 0.68$, $P < 0.001$) and Δunpleasantness ($r = 0.61$, $P < 0.001$), but the change in PAG-vmPFC connectivity (ΔPAG-vmPFC) had a negative correlation with the Δpain intensity ($r = -0.54$, $P < 0.001$) and Δunpleasantness ($r = -0.47$, $P < 0.001$) (**Fig. 6b, Supplementary Fig. 5a**). These results suggest that more substantial analgesic effect are paralleled by the more pronounced changes in these neural pathways. The mediation analysis revealed that ΔPAG-vmPFC connectivity partially mediates the relationship between ΔPAG-spinal connectivity and the analgesic effect. This was evident in both the Δpain intensity (indirect path = 0.01, P = 0.02, 95% C.I.= [0.004, 0.02], Fig. 6e) and Δunpleasantness (indirect path = 0.01, P = 0.05, 95% C.I.= [1.39e-4, 0.02], **Supplementary Fig. 5c**). These findings suggest that following Conventional TENS treatment, PAG-spinal connectivity not only directly impacts pain perception but also exerts an indirect influence by modulating PAG-vmPFC connectivity.

In the Acupuncture-Like TENS group **(Fig. 6c)**, a significant "order" effect was found for the PAG- S1 (left S1, ipsilateral to TENS stimulus) and PAG-spinal connectivity ($P < 0.05$, TFCE corrected), resulting from a significant decrease in PAG-S1 and increase in PAG-spinal for both TS (S1: $t_{(30)} = 2.88$, $P = 0.007$; spinal: $t_{(30)} = -2.94$, $P = 0.006$) and UTS (S1: $t_{(30)} = 2.78$, $P = 0.009$; spinal: $t_{(30)} = -2.20$, $P = 0.04$). The changes in PAG-S1 connectivity (ΔPAG-S1) had a significant positive correlation with Δpain intensity

(r = 0.31, P = 0.02) and Δunpleasantness (r = 0.29, P = 0.02), and the change in PAG-spinal connectivity (ΔPAG-spinal) had a negative correlation with Δpain intensity (r = -0.49, P < 0.001) and Δunpleasantness (r = -0.41, P < 0.001) (**Fig. 6d, Supplementary Fig. 5b**). These results also suggest that substantial analgesic effect are associated with pronounced changes in cortico-spinal pathways, however the PAG based associations seemed to be exactly opposite patterns for two TENS modes **(Fig. 6b vs Fig. 6d)**. Further, the mediation analysis revealed that ΔPAG-spinal connectivity fully mediates the relationship between ΔPAG-S1 connectivity and the analgesic effect. This was evident in both the Δpain intensity (indirect path = 0.68, P = 0.007, 95% C.I.= [0.26, 1.27], **Fig. 6f)** and Δunpleasantness (indirect path = 0.65, P = 0.02, 95% C.I.= [0.09, 1.20], **Supplementary Fig. 5d**). These findings suggest that following Acupuncture-Like TENS treatment, PAG-S1 connectivity can only indirect influence pain perception by modulating PAG-spinal connectivity.

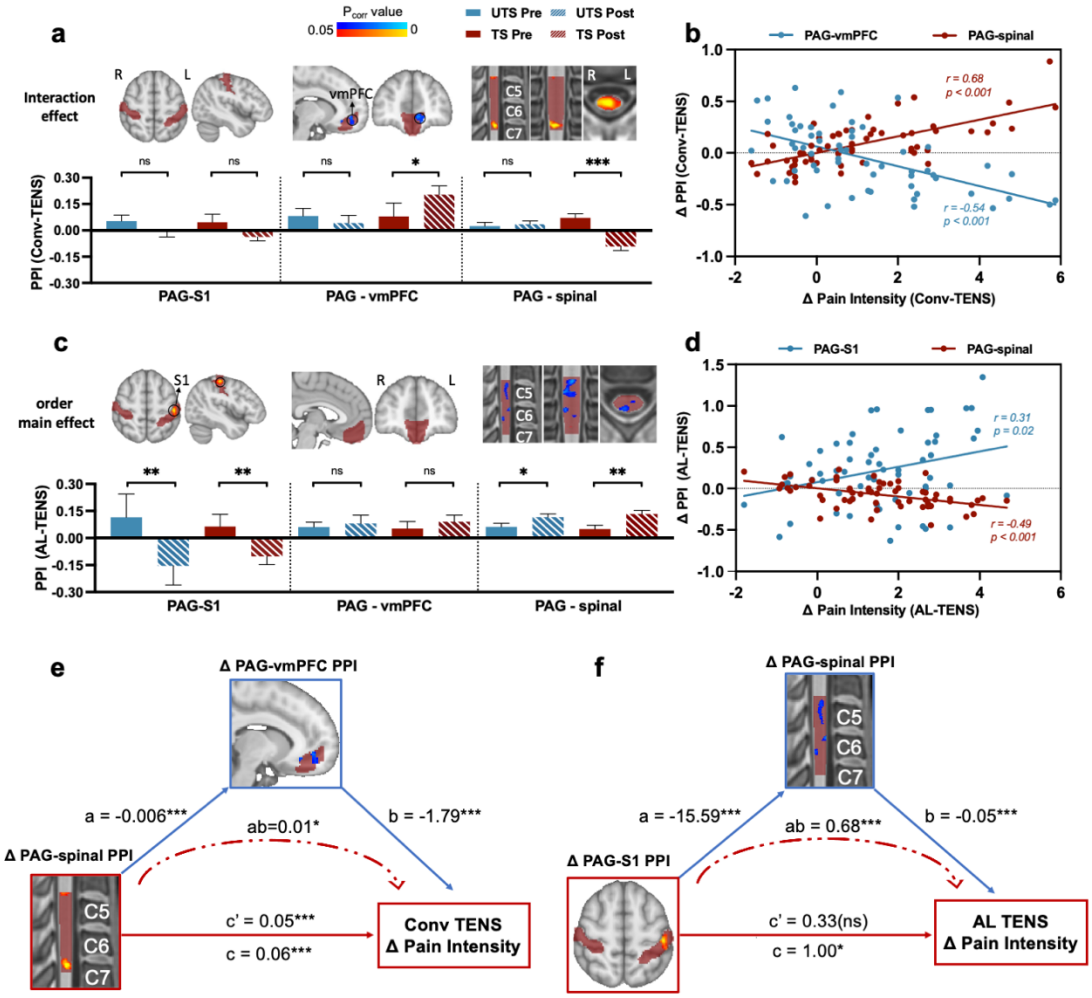

Figure 6. PAG-cortical and PAG-spinal connectivity modulate TENS analgesic effects. *(**a**) PAG-vmPFC and PAG-spinal connectivity exhibited a significant interaction in the Conventional TENS group (P < 0.05, TFCE corrected), with only TS showing significant differences. (**b**) Conventional TENS analgesic effect (Δpain intensity) positively correlated with ΔPAG-spinal connectivity (r = 0.68, P < 0.001) and negatively correlated with ΔPAG-vmPFC connectivity (r = -0.54, P < 0.001). (**c**) PAG-S1 and PAG-spinal connectivity demonstrated a main effect of "order" in the Acupuncture-Like TENS group (P < 0.05, TFCE corrected). (**d**) Acupuncture-like TENS analgesic effect (Δpain intensity) positively correlated with ΔPAG-S1 connectivity (r = 0.31, P = 0.02) and negatively correlated with ΔPAG-spinal connectivity (r = -0.49, P < 0. 001). (**e**) In the Conventional TENS group, ΔPAG-vmPFC connectivity partially mediated the effect of ΔPAG-spinal connectivity on Δpain intensity (indirect path = 0.01, P = 0.02, 95% C.I.= [0.004, 0.02]). (**f**) In the Acupuncture-Like TENS group, ΔPAG-spinal connectivity fully mediated the effect of*

*ΔPAG-S1 connectivity on Δpain intensity (indirect path = 0.68, P = 0.007, 95% C.I.= [0.26, 1.27]). Note: ΔPAG-spinal connectivity values were normalized by dividing each value by 100 for visualization. * P < 0.05; ** P < 0.01; *** P < 0.001; ns: not significant.*

Discussion

To the best of our knowledge, this is the first study to utilize simultaneous cortico-spinal fMRI to investigate the central analgesic mechanism of a noninvasive periphery neuromodulation technique — TENS. Through a three-way mixed-design combining the latest cortico-spinal fMRI with heat pain stimuli (**Fig. 1 a-c)**, we found that Conventional TENS primarily induces local analgesia effects on the treated side (**Fig. 2 and 3)**, while Acupuncture-Like TENS produces diffuse analgesic effects on both sides (**Fig. 2 and 4)**. A crucial discovery is the role of the PAG in TENS-induced analgesia, with activities in the dlPAG linked to Conventional TENS and vlPAG associated with Acupuncture-Like TENS (**Fig. 5**). Importantly, direct spinal inhibition (PAG-spinal connectivity) partially mediated by PAG-vmPFC connectivity leads to local analgesic effects in Conventional TENS. In contrast, a top-down diffuse noxious inhibition (PAG-S1 connectivity) fully mediated by PAG-spinal connectivity leads to diffusion analgesic effects in Acupuncture-Like TENS (**Fig. 6**). Our findings provide systematic neural evidence and a comprehensive understanding of the analgesic mechanisms induced by TENS.

These results were obtained by combining several recent advancements in simultaneous cortico-spinal fMRI to address the inherent difficulties in imaging a large area: simultaneous multi-slice imaging (SMS) with parallel image reconstruction to get shorter scan duration and less artifact aliasing; novel EPI distortion correction using reverse phase encoded B0s; robust physiological noise removal to increase tSNR and eliminate false positives; optimized analysis pipeline for separated brain and spinal cord images including preprocessing, co-registration, and group statistics, etc.

Understanding the analgesic mechanism of TENS is crucial for clinical applications of peripheral-based non-invasive neuromodulation. Two well-known and fundamental theories might be involved: gate control[23] and DNIC[43]. Gate control theory suggests that activating Aβ sensory afferents with tactile stimuli can inhibit nociceptive signals

395 at the spinal level. In contrast, the DNIC theory posits that nociceptive stimuli can
396 suppress pain by activating the descending pain modulation system[44], altering signal
397 input in the spinal cord. These theories involving systemic mechanisms encompass the
398 cortex, subcortical regions, and the spinal cord. Our study observed distinct disparities
399 in pain modulation between Conventional TENS and Acupuncture-Like TENS, evident
400 in both behavioral outcomes **(Fig. 2**) and cortico-brainstem-spinal BOLD responses and
401 couplings **(Fig. 3-4**), consistent with findings from animal studies[45,46].

402 Conventional TENS mainly provides pain relief limited to the directly treated area, as
403 seen by a significant reduction of pain at the TS as opposed to the UTS **(Fig. 2a,d**).
404 Corresponding to these behavioral observations, Conventional TENS was found to
405 significantly modulate activity in several regions activated by heat pain on the TS,
406 specifically in areas such as S2, vmPFC, PAG, RVM, and the spinal cord **(Fig. 3 and**
407 **Supplementary Fig. S2).** These findings robustly demonstrate the involvement of
408 supraspinal levels in Conventional TENS analgesia. Specifically, vmPFC, which is
409 involved in the emotional and cognitive aspects of pain and its modulation[47], was
410 influenced by Conventional TENS. Additionally, PAG and RVM, crucial brainstem
411 nuclei in the pain modulation system[33], also play a key role in this process. Recent
412 human studies have shown that Conventional TENS can increase functional
413 connectivity between PAG and lateral PFC[26], and increase cortico-spinal excitability,
414 which is indicated by motor evoked potentials (MEP) elicited by TMS[29]. Our results
415 **(Fig. 3)** support previous studies by showing that Conventional TENS works by
416 blocking opioid receptors in the RVM[48] and activating opioid receptors in the PAG[49].

417 Acupuncture-Like TENS demonstrated a more diffuse analgesic effect in behavioral
418 outcomes **(Fig. 2a, d**), which was evidenced by significant pain reduction observed on
419 both the TS and UTS, with a notable positive correlation between the two sides **(Fig.**
420 **2c, f**). Regarding BOLD responses, Acupuncture-Like TENS altered activations in a
421 widespread range of regions evoked by heat pain stimulation on both sides. These
422 regions include the right SMA, dACC, bilateral S1 and S2, left cerebellum, PAG, and
423 spinal cord **(Fig. 4)**. A previous EEG study also revealed that Acupuncture-Like TENS
424 could induce the spontaneous activity state changes within the sensory-motor cortex
425 (S1/M1), and increase functional connectivity between S1 and the medial PFC[13].
426 Furthermore, other research has shown that after Acupuncture-Like TENS treatment in

427 carpal tunnel syndrome patients, there was a significant decrease in the activation
428 intensities of S2, M1, bilateral SMA, and other regions compared to baseline[27]. Recent
429 studies on the cortico-spinal mechanisms of conditioned pain modulation (CPM) also
430 demonstrate the importance of S2[50].
431
432 An interesting finding is the differential S2 responses to TENS modes: Conventional
433 TENS specifically reduced ipsilateral S2 pain activation **(Fig. 3b)**; in contrast,
434 Acupuncture-Like TENS led to a bilateral decrease in S2 pain activation **(Fig. 4c)**. S2
435 encodes the intensity and location of pain[51], but is also involved in higher-order
436 functions, including sensorimotor integration, synthesis of bilateral information,
437 attention, learning, and memory[52-54]. Animal studies have demonstrated that unilateral
438 tactile stimulus could modulate neuronal activity in somatosensory cortices of the
439 ipsilateral hemisphere[55,56], which may support Conventional TENS as a form of tactile
440 stimulation, reducing ipsilateral S2 activation. Bilateral S2 is involved in pain
441 processing across both humans and animals[57], the decrease in bilateral S2 activation
442 further substantiates the widespread analgesic effect induced by Acupuncture-Like
443 TENS.

444 The response patterns across various brain regions under different TENS modes may
445 depend on different descending pain modulation pathways[35,58]. Both TENS engage the
446 PAG in their analgesic processes (**Fig. 3d, 4d and Supplementary Fig. 4b**).
447 Furthermore, The dlPAG is more actively involved in Conventional TENS, while the
448 vlPAG is more prominent in Acupuncture-Like TENS **(Fig. 5)**. The PAG receives and
449 transmits cortical inputs to the RVM and other key regions in the descending pain
450 modulation system[59]. This complex role is highlighted in various studies, including
451 those on opioid analgesia[35], placebo analgesia[60,61], attention-driven analgesia[36,62], and
452 expectations of pain response[63], all indicating intricate interactions within a broad
453 network. Moreover, distinct subregions within the PAG contribute differently to pain
454 modulation[64]. Preclinical studies have shown that opioid-mediated analgesia involves
455 neurons in the vlPAG, while non-opioid analgesia is associated with neurons in the
456 lPAG and dlPAG[65-67]. This differentiation suggests that the analgesic effect of
457 Conventional TENS might be due to spinal-driven inhibition rather than opioid-

458 mediated descending modulation. Conversely, Acupuncture-Like TENS's efficacy
459 seems to be linked to opioid-related descending modulation.

460 Focusing solely on the activations of brain and spinal cord regions seems insufficient;
461 taking advantage of innovative cortico-spinal imaging, we further examine functional
462 interactions along the central nervous system[68]. The functional connectivity between
463 the PAG-cortical and PAG-spinal induced analgesic effects provides crucial insights
464 into the PAG's role in pain modulation. We find that PAG-vmPFC connectivity showed
465 significant alterations following Conventional TENS application **(Fig. 6a)**, and these
466 changes correlated with analgesic effects **(Fig. 6b)**. Enhanced coupling between the
467 PFC and PAG has been observed in placebo analgesia[69,70]; furthermore, a more
468 substantial placebo analgesic effect is associated with increased coupling strength[70].
469 Previous animal studies have demonstrated that subpopulations of mPFC neurons
470 project to the PAG, specifically the dlPAG[71,72]. In the Acupuncture-Like TENS group,
471 changes in PAG-S1 were correlated with analgesic outcomes **(Fig. 6c, d)**. Existing rs-
472 fMRI connectivity between the vlPAG and S1[66] is related to top-down pain
473 modulation[73,74], and the vlPAG has efferent connections with the spinal cord, which is
474 also related to opioid-mediated analgesia[75].

475 Additionally, significant alterations in PAG-spinal connectivity were observed
476 following both TENS treatments, with these changes correlating with analgesic effects
477 (**Fig. 6b, d**). However, the direction of these changes differed between modes: in the
478 Conventional TENS group, connectivity shifted from positive to negative, whereas in
479 the Acupuncture-Like TENS group, positive connectivity was enhanced post-treatment
480 (**Fig. 6a, c**). Neural projections between the PAG and spinal cord are well-established[76],
481 with their connectivity strength linked to pain intensity[35,77]. Positive connectivity,
482 where activation in one area boosts activity in another, indicates synergy, while
483 negative connectivity suggests inhibition, as activation in one region diminishes
484 activity in another[78]. In the Conventional TENS group, reversing positive to negative
485 PAG-spinal connectivity may signify spinal-driven inhibition, reducing pain signal
486 transmission. Conversely, enhanced positive PAG-spinal connectivity in the
487 Acupuncture-Like TENS group points to a systemic pain modulation mechanism,
488 possibly opioid-mediated descending modulation, where increased connectivity
489 enhances pain inhibitory pathways.

Our mediation results further illustrate that Conventional TENS-induced analgesia through both direct spinal inhibition (PAG-spinal connectivity) and descending modulation pathways (PAG-vmPFC connectivity) (**Fig. 6e**). In contrast, Acupuncture-Like TENS's diffusion analgesic effects appear to be fully induced by descending DNIC (PAG-S1 connectivity fully mediated by PAG-spinal connectivity) (**Fig. 6f**). This further explicates that the strongest localized (i.e. treated side) behavioral analgesic effects induced by Conventional TENS (**Fig. 2 b,e**) result from the synergistic action of dual pathways, with the descending modulation pathway also eliciting non-significant changes in pain-induced perceptions and cortico-spinal activations in the UTS. Conversely, the analgesic effects elicited by Acupuncture-Like TENS exhibit diffuse and consistent characteristics across both subjective perceptions and cortico-spinal activations and connectivity, serving as compelling evidence of the DNIC's effectiveness. These observations provide crucial insights into the neurobiological mechanisms underpinning the efficacy of these two TENS modes.

This study used an effective behavioral paradigm and simultaneous cortico-spinal imaging technology to systematically investigate the analgesic effects and cortico-brainstem-spinal mechanisms of TENS, a typical peripheral neuromodulation method. We observed differences in the analgesic effects of the two TENS modes at the behavioral level and confirmed distinct mechanisms by examining PAG-vmPFC, PAG-S1, and PAG-spinal connections. Most importantly, we demonstrated the crucial role of spinal inhibition and descending pain modulation in Conventional TENS analgesia and descending pain modulation in Acupuncture-Like TENS analgesia. Our results support TENS for pain management and open avenues for exploring cortico-spinal mechanisms in other neuromodulation techniques like TMS, tDCS, and spinal cord stimulation (SCS). However, this study has limitations, primarily using young healthy subjects for experimental acute pain, without utilizing chronic pain models (e.g., capsaicin) in a larger sample and across a wider age range, or involving TENS analgesia in actual patients. Future research will delve deeper into the analgesic effects of TENS on various chronic pain patients, aiming to understand its clinical mechanisms better.

Materials & Methods

Participants. Ninety-five healthy participants were invited to participate in this study. All participants were right-handed, had no history of chronic pain, mental illness, or analgesics, and had not previously undergone TENS treatment. Due to equipment failure, three participants were unable to complete the study. Thus, the final analysis included ninety-two participants (50 females, age (mean ± SD) = 21.9 ± 3.23). The study was conducted in accordance with the Declaration of Helsinki and received approval from the Ethics Committee of the Institute of Psychology at the Chinese Academy of Science. All participants provided informed written consent, underwent MRI safety screening of scanning, and were fully debriefed about the deception used in the experiment after its completion. Participants received a compensation of 200 RMB for their participation.

Experimental procedure. Participants were documented written informed consent, demographic information, and MRI safety screening during the preparation phase. After explaining the experimental procedure and rating guidelines, they practiced for exposure to painful stimuli, followed by the calibration of heat pain stimulation and quantitative sensory testing (QST) before the experiment. Pain cognition and emotion assessments were also conducted through questionnaires to exclude group differences. The experiment was divided into three sessions: pre-TENS, TENS treatment (conducted outside the MRI room), and post-TENS (**Fig. 1a),** with simultaneous cortico-spinal structural and heat pain task-based functional MRI scans performed during the pre- and post-TENS sessions.

Sensory stimulation

Transcutaneous nerve electrical stimulation (TENS). The TENS treatment was delivered using a multichannel electrical stimulator (SXC-4A, Beijing Sanxia Technology Co., Ltd., China)[14]. Two pairs of electrodes (diameter: 16 mm; interelectrode distance: 3 cm) were attached to the C5~C6 dermatomes in the ventrolateral part of the left forearm (treatment side) **(Fig. 1c)**.

The electrical stimuli in TENS consisted of a series of constant-current square-wave pulses, with the TENS treatment parameters varying across experimental groups and

each stimulation lasting 30 minutes[11,13,14,79] (**Fig. 1a**). The Conventional TENS group received high-frequency stimulation at 100 Hz, with a 2000 μs pulse width and intensity set at 6.04 ± 1.44 mA, inducing a strong but nonpainful tingling sensation without causing muscle contractions. The Acupuncture-Like TENS group received low frequency stimulation at 4 Hz, with a 4000 μs pulse width and higher intensity of 7.00 ± 1.42 mA, set to elicit severe but tolerable pain and muscle twitching, akin to acupuncture needle sensation. The sham TENS group was informed of receiving faint electrical stimulation, but no actual current was delivered. The stimulation intensity between the Conventional TENS group and the Acupuncture-Like group was significantly different ($t_{(59)} = 2.62$, $P = 0.01$; **Fig. 1e**), ensuring a clear distinction between "low intensity" for Conventional TENS and "high intensity" for Acupuncture-Like TENS.

This study was single-blinded, and the experimenter was aware of the group assignments to set the treatment parameters, but the participants were not. To minimize the placebo effect and other possible interference factors, such as expectations, we did not mention that the study was related to analgesia, nor was electrical stimulation presented as an intervention measure during the experiment. The TENS procedure required all participants to sit quietly, pay attention to the stimulation position, and feel the electrical stimulation. All participants were told, "An electrical stimulation will be continuously applied to your left forearm for the next 30 minutes. Please close your eyes and feel this stimulation".

The TENS stimulation intensity was determined using the methods of limit[80]. The Conventional TENS started from 2 mA and increased by 0.5 mA each time until the participants reported "strong tingling but painless," which was the initial stimulation intensity. The Acupuncture-Like TENS started at 5 mA and increased until a tolerable pain level was reached, which was taken as the initial stimulation intensity. The stimulation intensity was adjusted every 5 minutes based on the participant's subjective feelings during the TENS procedure, and the stimulation intensity and subjective feelings were recorded.

Heat pain stimulation. Heat pain stimulation was delivered using a Pathway device (Medoc Ltd, Ramat Yishai, Israel) with a 573 mm^2 (diameter of 27 mm) CHEPS

thermode, targeting the C5~C6 dermatomes on participants' both forearms. The thermode was positioned next to the TENS electrodes without overlap **(Fig. 1c)**. Uniform pressure application was ensured by adjusting the length of the thermode's Velcro strap.

Two runs of heat pain stimulation comprising 15 trials on each forearm were conducted with a pseudorandom order to balance side placement. The heat pain stimulation pattern began at a baseline of 32 °C, was quickly ramped to the target temperature at 40°/s, was held for 3 seconds, and then returned to baseline at the same rate. Participants used a button box to rate pain intensity and unpleasantness on a Numeric Rating Scale (NRS) from 0-10, 12s after thermal stimulation. The scale for pain intensity had "no feeling" at 0, "just pain" at 4, and "unbearable pain" at 10. The unpleasantness scale ranged similarly from "no unpleasantness" at 0 to "extreme unpleasantness" at 10. Each rating was displayed for 5s, with a 12-15s randomized inter-trial interval**(Fig. 1b)**.

The target temperature for heat pain stimulation was set at each participant's subjective pain intensity of 7/10 on the NRS. Using the methods of limit[80], stimuli were randomly applied to either side, with temperatures ranging from 44~47°C in 0.5°C increments until a consistent pain intensity rating of 7 was achieved. No significant temperature differences were found among the three groups (Conv-TENS: 45.75 ± 1.35 °C (mean ± SD); AL-TENS: 45.85 ± 1.76 °C; Sham-TENS: 46.16 ± 1.51 °C; $F_{(2,89)} = 0.58$, $P = 0.56$).

Questionnaires and QST. The study employed a range of questionnaires to assess pain cognition and emotion. These included the Pain Sensitivity Questionnaire (PSQ)[81], Pain Anxiety Symptom Scale (PASS)[82], Pain Catastrophizing Scale (PCS)[83], Pain Vigilance and Awareness Questionnaire (PVAQ)[84], State-Trait Anxiety Inventory (STAI)[85], Beck Depression Inventory (BDI)[86], Interpersonal Reactivity Index (IRI)[87,88], and Fear of Pain Questionnaire (FPQ)[89].

In addition, the QST protocol[90] was utilized. Mechanical tactile thresholds were determined using the Semmes–Weinstein filaments (Touch-Test ™20 Piece Kit, North Coast Medical, Inc., USA), and electrical tactile and pain thresholds were determined using the multichannel electrical stimulator, all targeting the C5~C6 dermatome of the

left forearm. The Pathway device with a 9cm^2 ATS thermode was used for heat and cold pain threshold tests on the ventrolateral C5~C6 dermatomes of both forearms.

MRI data acquisition. The imaging data were collected using a 3T MRI scanner (Siemens Prisma, Erlangen, Germany) at Beijing Tiantan Hospital, which was equipped with a standard 64-channel head and neck coil. Participants were carefully positioned in the scanner, with a foam pad used to elevate the head and straighten the cervical spine, minimizing potential image distortion and physiological noise. Additional foam pads were placed on either side of the participant's head, and neck braces were used to limit head and neck movements. Sponge earplugs were provided to protect the participant's hearing.

A modified cortico-spinal fMRI protocol, based on the Siemens SMS-EPI sequence, was employed to capture the brain and cervical cord's BOLD response simultaneously **(Fig. 1e).** Specifically, FOV was expanded to 192×192mm^2, and 70 slices (each 4 mm thick) were scanned to cover the whole brain and cervical spinal cord (C1-C7). A 3D shimming volume (37 × 62 × 267 mm^3), perpendicular to the acquisition slab, was added to focus specifically on the brainstem and cervical cord areas. In addition, the phase coding direction was set from posterior to anterior (P→A), the flip angle was set at 80°, the FOV phase was set at 100%, and the in-plane resolution was set at 1.5 × 1.5 mm^2. To expedite the imaging process, we implemented a simultaneous multiband combined GRAPPA parallel imaging method[91], using an interleaved multi-slice mode and acceleration factor of 2 for both phase encoding and slice selection. This approach resulted in a repetition time (TR) of 2680 ms and an echo time (TE) of 27 ms. In total, 230 volumes were scanned.

To rectify the distortion, particularly around the cervical spine, induced by the extensive FOV and magnetic field inhomogeneities, we used the TOPUP tool from FSL in conjunction with two B0 images (diffusion acquisition with b=0) with opposing phase encoding directions (for methodological details, refer to fMRI data preprocessing). A pair of B0 images (TR: 7500 ms, TE: 87 ms, phase encoding of A→ P and P→A) were acquired using a 2D SP-EPI sequence, maintaining the same FOV, resolution, echo spacing, acceleration, and shimming as fMRI.

The high-resolution (1 × 1 × 1 mm^3) T1-weighted anatomical images were acquired using a 3D MPRAGE sequence[92] with the following parameters: sagittal slice orientation, TR: 2300 ms, TE: 2.28 ms, TI: 900 ms, FOV: 192 × 288 × 288 mm^3, FOV phase: 100%, flip angle: 8°.

Participants wore a pulse oximeter and respiratory belt to record respiratory and cardiac data at a frequency of 400Hz under the Siemens Physiologic Monitoring Unit (PMU) during fMRI scanning. Physio log files were used to generate physiological noise regressors in the data processing procedure. The E-prime 2.0 was utilized to control the experimental stimulus presentation and record behavioral ratings.

Behavioral data analysis. The statistical analyses of the behavioral data were performed using the open-source software *jamovi* 1.2 (The *jamovi* project, 2020, https://www.jamovi.org). One-way ANOVA was used to analyze the demographic data, questionnaires, and QST indices to exclude between-group variance. The mean pain intensity and unpleasantness ratings for each block were calculated for each participant. A 3 (group: Conventional, Acupuncture-Like, Sham) × 2 (side: TS; UTS) × 2 (order: pre-TENS, post-TENS) mixed-factorial ANOVA was used to estimate the main effect and interactions of behavioral data. Post hoc within-group 2 "side" × 2 "order" repeated measures ANOVA and paired t-tests were subsequently performed. For the results that were not significant, we conducted Bayesian ANOVA and post hoc t-tests to enhance the robustness of the findings.

In order to quantify the analgesic effect of TENS, we calculated the changes (Δ) in both pain intensity and unpleasantness of each participant, derived from the mean pre-TENS rating minus the mean post-TENS rating. These metrics enabled us to gauge the effectiveness of the TENS treatment on subjective pain perception. Subsequently, a 3 (group: Conventional, Acupuncture-Like, Sham) × 2 (side: TS, UTS) mixed-factorial ANOVA was employed to explore the variations in Δpain intensity and Δunpleasantness between the three different TENS groups. Post hoc independent-sample t-tests were conducted to further examine the differential analgesic effects between groups, while paired t-tests were used to compare the TS with the UTS within each group. A Pearson correlation analysis was also conducted to probe the relationship between the analgesic effects (both Δpain intensity and Δunpleasantness) on the TS and

672 the UTS. This analysis enabled us to understand whether the analgesic effects were
673 localized to the treated side or extended to the untreated side. $P<0.05$ was considered
674 as statistically significance for all behavioral analyses.

675 **MRI data preprocessing**. Imaging data were processed with FSL 6.0.6.5[93] (FMRIB
676 software library) and SCT 5.6[94] (Spinal Cord Toolbox). Visual quality control was
677 performed after each step of processing to ensure the accuracy of the results. Because
678 the brain and the spinal cord significantly differ structurally, and the cortico-spinal
679 acquisition was heavily influenced by the distortion and physiological noise, specific
680 data processing steps and statistical methods were implemented separately for the brain
681 and the spinal cord, although they adopted similar data processing flows.

682 **Structural image preprocessing**. The cortico-spinal T1-weight structural image was
683 firstly corrected for field bias and reoriented to the standard (MNI) orientation using
684 *fsl_anat* (FSL's atomical image processing pipeline) and then was divided into the brain
685 and the cervical cord along the end of the brainstem. As for the brain section, brain
686 tissues were extracted using the Brain Extraction Tool (BET)[95] **(Fig. 1d)** for the
687 subsequent registration of functional images. Each brain image was checked visually
688 and adjusted manually for inadequate automatic skull stripping.

689 We used the Spinal Cord Toolbox to process the structural image of the spinal cord
690 section. Initially, the centerline was detected, followed by automatically generating a
691 binary spinal cord mask using the *sct_deepseg_sc* in the SCT. The segmentation quality
692 was checked and adjusted manually in case of insufficient segmentation. Subsequently,
693 to identify spinal cord segments, eight intervertebral disc points ranging from C1 to C8
694 were manually marked on the original structural image using the *sct_label_utils* in the
695 SCT **(Fig. 1d)**. Spatial registration of the spinal cord using the *sct_register_to_template*
696 in the SCT. This registration process includes three main steps. Firstly, the spinal cord
697 was straightened using the segmentation binary mask. This is followed by aligning the
698 vertebrae of the structural image with the template, using labels along the intervertebral
699 disc points. The final step involves iterative slice-wise non-linear registration of the
700 individual's structural image with the PAM50 standard template ($0.5 \times 0.5 \times 0.5$ mm^3)[96].
701 These steps produce warp fields, enabling bidirectional transformations between the

standard template and the individual structural image. These transformations are crucial for accurate alignment in subsequent fMRI registration processes.

Functional image preprocessing. First, the physiological noise model (PNM) toolbox of FSL was used to estimate respiratory and cardiac noise from the original cortico-spinal fMRI images. This process generated 32 slice-specific regressors for both the brain and spinal cord[97-99]. Subsequently, we applied a linear regression to denoise the original fMRI data. Simultaneous cortico-spinal EPI images with large FOV have apparent distortion[100], and traditional correction methods, such as a double-echo gradient echo field map, proved inadequate in rectifying these distortions. Drawing inspiration from the diffusion distortion correction method, we opted for a different approach in the second stage, where B0 images with reverse phase encoding directions were used through the TOPUP tool[101] (a tool in FSL for estimating and correcting susceptibility-induced distortions) to correct the EPI distortions[102] **(Fig. 1e)**. The expanded FOV acquisition with multiband-interleaved sequence required a long TR of 2.68 seconds, which would inherently lead to a temporal offset of multiple slices. We utilized the *slicetimer* function in FSL to reconcile these temporal discrepancies as the third step[103]. This process allowed the signal responses across all slices, from the spinal cord to the cortex, to appear as if they were acquired simultaneously.

Upon completion of physiological noise regression, distortion correction, and slice timing correction, we partitioned the images along the Z-dimension, delineating the lower boundary of the brainstem. This segmentation allowed for the independent preprocessing of the brain and the cervical spinal cord, thereby tailoring the approach to the unique characteristics of these distinct anatomical regions.

Brain fMRI preprocessing. The brain section of fMRI data was preprocessed using the FMRI Expert Analysis Tool (FEAT, part of the FSL tool). This analysis began with motion correction performed by MCFLIRT[104], followed by extraction of brain tissue signals using the BET. We then applied spatial smoothing to each volume with a Gaussian kernel featuring a 5-mm full-width at half-maximum (FWHM), and high-pass temporal filtering (cutoff: 100 s) was employed to eliminate low-frequency drifts. We used FILM (FMRIB's improved linear model)[101] to estimate autocorrelation and prewritten each voxel's time series. We co-registered the fMRI images with each

733 participant's T1-weighted structural image using the boundary-based registration
734 method (BBR). As a final step, we spatially normalized the co-registered images to the
735 MNI-152 2-mm standard brain template utilizing the nonlinear registration tool
736 FNIRT[105].

737 ***Spinal cord fMRI preprocessing.*** The spinal cord section of fMRI data was
738 preprocessed using the SCT and FSL. The first step involved automatic identification
739 of the spinal cord's centerline (*sct_get_centerline* in the SCT), enabling the generation
740 of a 3D binary mask with a 35mm diameter（*sct_create_mask* in the SCT). Following
741 this, we corrected slice-wise motion with the *sct_fmri_moco* tool, confining translations
742 within the 2D plane. Subsequently, spatial smoothing was performed along the X and
743 Y dimensions, employing a Gaussian kernel with an FWHM of 3 mm (*sct_maths* in the
744 SCT). The final step in this pipeline involved the application of high-pass temporal
745 filtering (sigma = 100 s) to remove low-frequency drifts. Furthermore, we manually
746 drew the segmentation mask of the spinal cord from the motion-corrected functional
747 mean image for registration **(Fig. 1e).** The motion-corrected functional images were
748 registered to the T1-weighted image using non-rigid transformations
749 (*sct_register_multimodal* in the SCT). Lastly, the warping fields from individual
750 structural to the template and individual functional to structural were concatenated,
751 resulting in the functional to template transformation (*sct_apply_transfo* in the SCT).
752 To validate the accuracy of our registration to the PAM50 template, we have presented
753 the results of this procedure in **Supplementary Fig. 1**, demonstrating the precise
754 correspondence between the normalized functional images and the template.

755 **Statistical analysis of fMRI data**

756 ***First-level analysis***. The fMRI data analysis was performed separately for the brain and
757 spinal cord in FEAT under the framework of GLM[106]. The first-level design matrix for
758 the brain and spinal included explanatory variables (EVs) of the pain stimulus, rating
759 blocks, and time derivatives. The voxelwise top 10% of the strongest signal in
760 cerebrospinal fluid (CSF) in each spinal slice was extracted as an additional nuisance
761 regressor included in the spinal cord first-level GLM statistical analysis. Following the
762 initial analysis, the contrast of parameter estimates (COPE) for pain stimulation derived
763 from the spinal cord section was registered to the PAM50 standard space for group-

level statistical analysis using the previously identified warp field images (*sct_apply_transfo* in the SCT).

Group-level analysis. In this study, we applied a mixed-effect approach[107,108] (FLAME, FMRIB's Local Analysis of Mixed Effects) to conduct group-level statistical analyses of the whole brain, including group average, difference, and PPI). Whole brain analyses were performed with a cluster-wise correction ($Z > 3.1$, $P < 0.05$). However, detecting activation in the brainstem presents a significant challenge due to its susceptibility to physiological noise and artifacts[109], the small size, and the relative distance from signal detectors in the head coil. Moreover, Gaussian random field theory-based FWE corrections are unsuitable for tiny cylindrical structures such as the spinal cord, possibly leading to increased false negatives[110]. Consequently, we opted for nonparametric permutation tests[111] (*randomise*, part of FSL toolbox) for group analysis of the brainstem and spinal cord. Our focus was on a whole brainstem mask derived from the probabilistic Harvard-Oxford subcortical structural atlas[112] and threshold at 70%, as well as the C6 segment in the PAM50_cord template[96]. The nonparametric results were subjected to TFCE correction ($p < 0.05$, threshold-free cluster enhancement[113] after 10,000 permutations[114].

We obtained group average activities of heat pain on both sides in the pre-TENS session using a one-sample t-test. Then, the repeated measures ANOVA, featuring a 2 (side: TS, UTS) × 2 (order: pre-TENS, post-TENS) design, was independently applied to each group with the brain and spinal section. Data were arranged as UTS-pre, UTS-post, TS-pre, and TS-post. For the main effect of "order", we used contrasts '1 1 -1 -1' and '-1 -1 1 1', and for the main effect of "side", we used contrasts '1 -1 1 -1' and '-1 1 -1 1'. To explore the interaction between "order" and "side", contrasts '-1 1 1 -1' and '1 -1 -1 1' were employed. Our focus was on the interaction effects [(TS-pre minus TS-post) vs. (UTS-pre minus UTS-post)] and the main effects of "order". It is important to note that pain is typically represented contralaterally in the brain[115]. Therefore, heat pain stimuli applied to the left and right forearms can lead to different lateralization patterns of brain activation. This aspect is essential to address potential biases in lateralized brain responses, which might arise from differences in nociceptive stimulation on each side[40,41]. To mitigate this in our analysis, particularly in the ANOVA, we swapped the X dimension (*fslswapdim* in the FSL) of each participant's normalized COPE and

VARCOPE images with the right-side session (UTS-pre and UTS-post) for ANOVA, ensuring a balanced representation of the stimuli from both sides.

In the subsequent analysis, we extracted the PEs from regions with significant interaction effect in the Conventional TENS group (S2, vmPFC, PAG, RVM, and C6 of spinal) and regions with significant main effect of "order" in the Acupuncture-Like TENS group (S1, SMA, dACC cluster, S2, PAG, vmPFC, and C6 of spinal). To understand the direction of changes, post hoc paired t-tests (pre-TENS vs. post-TENS) were performed on these extracted PEs **(Fig. 3, 4**). The ANOVA results revealed that PAG was involved in the Conventional and Acupuncture-Like TENS analgesia process. We specifically aimed to investigate the correlation between the change in PAG activity (pre-TENS minus post-TENS, denoted as ΔPAG) and behavioral analgesic effects (Δpain intensity) across different test sides (TS and UTS) in the two groups. Our analysis entailed separate linear regression for each group, with Δpain intensity as the dependent variable and ΔPAG activity as covariates; test sides were included as categorical factors. If test sides influenced the dependent variable, we examined the correlation between Δpain intensity and ΔPAG activity under TS and UTS conditions **(Fig. 5**).

Psycho-physiological interaction and Mediation Analysis. We performed a psycho-physiological interaction (PPI) analysis with the PAG as a seed to explore the functional interaction along the cortico-brainstem-spinal endogenous analgesia pathway. For the Conventional and Acupuncture-Like TENS group, we defined PAG functional masks from regions with significant ANOVA effects **(Fig. 5 a, b**), and extracted their mean time courses from individual preprocessed images. The first-level PPI model, applied separately to the brain and spinal cord, included four regressors: psychological regressor (pain stimulus), physiological regressor (PAG time course), their interaction, and rating blocks. The CSF nuisance regressor was added to the spinal cord, the same as the GLM model. Individual parameter estimation images for PPI were then taken to the higher-level 2 (side: TS, UTS) × 2 (order: pre-TENS, post-TENS) repeated measures ANOVA for two groups. We swapped the X dimension of each subject's normalized right-side condition COPE and VARCOPE images for further group ANOVA comparisons.

We defined the regions of the bilateral S1, vmPFC, and C5~6 spinal cord segments as target regions for small-volume corrections. Specifically, the S1 mask was selected from the Harvard-Oxford Cortical Structural Atlas[112], focusing on the postcentral gyrus with a threshold set at 70%; the vmPFC mask was identified by selecting the frontal medial cortex, applying a threshold of 90%. The C5~6 segments mask was chosen from the PAM50_cord template[96] for the spinal cord. In the subsequent analysis, we extracted the connectivity values from regions with significant interaction effect in the Conventional TENS group (PAG-vmPFC and PAG-spinal cord) and regions with significant main effect of "order" in the Acupuncture-Like TENS group (PAG-S1 and PAG-spinal cord). Post hoc paired t-tests (pre-TENS vs. post-TENS) were performed on these connectivity values to understand the direction of changes.

We further delved into the relationship between the significant PAG-related connectivity changes (pre-TENS minus post-TENS, ΔPAG-S1, ΔPAG-vmPFC, and ΔPAG-spinal cord) and the behavioral analgesic effects within two TENS groups. In the Conventional TENS group, we specifically focused on ΔPAG-vmPFC and the ΔPAG-spinal cord connectivity, and in the Acupuncture-Like TENS group, we specifically focused on ΔPAG-S1 and ΔPAG-spinal cord connectivity. Subsequently, these Δconnectivity values were subjected to Pearson's correlation analysis with Δpain intensity and Δunpleasantness.

In the following step, we constructed a GLM mediation analysis using the 'jAMM' package in the *jamovi* to inspect the potential mediation effect of Δconnectivity and analgesic effect (Δpain intensity and Δunpleasantness) across each group. We applied a bootstrapping approach with 1,000 iterations to estimate the indirect effect and its 95% confidence interval. In our model, ΔPAG-cortical and ΔPAG-spinal connectivity were positioned as the independent or mediator variable, while the analgesic effect (Δpain intensity and Δunpleasantness) was set as the dependent variable. The mediation model considered both direct and indirect effects. The direct effect represents the influence of the independent variable on the dependent variable, bypassing the mediator. In contrast, the indirect effect signifies the impact of the independent variable on the dependent variable through the mediator.

Acknowledgments

Y.K. is supported by the National Key R&D Program of China (No.2022YFC3500603), National Natural Science Foundation of China (82072010), Beijing Natural Science Foundation (IS23108); L.H. is supported by the National Natural Science Foundation of China (32071061) and Beijing Natural Science Foundation (JQ22018), M.Z. is supported by the National Natural Science Foundation of China (82030121 and 32100861); Y.L. is supported by the National Natural Science Foundation of China (82330057), Capital Medical Science Innovation Center Scientific Research Pioneering Project (NO.CX23YQ06), Capital Health Development Scientific Research Special Project of Beijing Municipal Health Commission (NO.2022-1-2042), The Cross-Research Project of Beijing Science and Technology Star Program (NO.H020620471020), Ministry of Science and Technology of China-National Key Research Project (NO.2022YFC2009904), and Beijing Hospital Management Center-Climb Plan (No. DFL20220503). Thanks to Jiyuan Wang, Guangyue Tian, Jiahui Zhong, and others for their support in data collection and methodology. Thanks to Siemens Health engineers who assisted in sequence commissioning and the engineers who repaired the experimental equipment.

References

1. Cohen, S.P., Vase, L. & Hooten, W.M. Chronic pain: an update on burden, best practices, and new advances. *Lancet* **397**, 2082-2097 (2021).
2. Yong, R.J., Mullins, P.M. & Bhattacharyya, N. Prevalence of chronic pain among adults in the United States. *PAIN* **163**(2022).
3. Volkow, N.D. & Blanco, C. The changing opioid crisis: development, challenges and opportunities. *Mol Psychiatry* **26**, 218-233 (2021).
4. Davis, C.S., Lieberman, A.J., Hernandez-Delgado, H. & Suba, C. Laws limiting the prescribing or dispensing of opioids for acute pain in the United States: A national systematic legal review. *Drug Alcohol Depend* **194**, 166-172 (2019).
5. Groenewald, C.B., Murray, C.B., Battaglia, M., Scaini, M.S. & Quinn, P.D. Prevalence of pain management techniques among adults with chronic pain in the United States, 2019. *JAMA Network Open* **5**, e2146697-e2146697 (2022).
6. Knotkova, H., *et al.* Neuromodulation for chronic pain. *Lancet* **397**, 2111-2124

(2021).

7. Vance, C.G., Dailey, D.L., Rakel, B.A. & Sluka, K.A. Using TENS for pain control: the state of the evidence. *Pain Manag* **4**, 197-209 (2014).

8. Johnson, M.I., Paley, C.A., Jones, G., Mulvey, M.R. & Wittkopf, P.G. Efficacy and safety of transcutaneous electrical nerve stimulation (TENS) for acute and chronic pain in adults: a systematic review and meta-analysis of 381 studies (the meta-TENS study). *BMJ Open* **12**, e051073 (2022).

9. Vance, C.G.T., Dailey, D.L., Chimenti, R.L., Van Gorp, B.J., Crofford, L.J. & Sluka, K.A. Using TENS for Pain Control: Update on the State of the Evidence. *Medicina (Kaunas)* **58**, 1332 (2022).

10. Brenner, B., Ericson, T. & Kohan, L. Advances in Non-Invasive Neuromodulation. *Curr Pain Headache Rep* **26**, 709-717 (2022).

11. Gibson, W., Wand, B.M., Meads, C., Catley, M.J. & O'Connell, N.E. Transcutaneous electrical nerve stimulation (TENS) for chronic pain-an overview of Cochrane Reviews. *Cochrane Database of Systematic Reviews* (2019).

12. Borges, M.R., de Oliveira, N.M.L., Antonelli, I.B.S., Silva, M.B., Crema, E. & Fernandes, L.F.R.M. Transcutaneous electrical nerve stimulation is superior than placebo and control for postoperative pain relief. *Pain Management* **10**, 235-246 (2020).

13. Peng, W.W.*, et al.* Neurobiological mechanisms of TENS-induced analgesia. *Neuroimage* **195**, 396-408 (2019).

14. Bi, Y., Wei, Z., Kong, Y. & Hu, L. Supraspinal neural mechanisms of the analgesic effect produced by transcutaneous electrical nerve stimulation. *Brain Struct Funct* **226**, 151-162 (2021).

15. Ottoson, D. & Lundeberg, T. *Pain treatment by transcutaneous electrical nerve stimulation (TENS): A practical manual*, (Springer Science & Business Media, 2012).

16. O'Connell, N.E., Marston, L., Spencer, S., DeSouza, L.H. & Wand, B.M. Non-invasive brain stimulation techniques for chronic pain. *Cochrane database of systematic reviews* (2018).

17. Dailey, D.L.*, et al.* Transcutaneous electrical nerve stimulation reduces pain, fatigue and hyperalgesia while restoring central inhibition in primary

922 fibromyalgia. *Pain* **154**, 2554-2562 (2013).
923 18. DeSantana, J.M., Da Silva, L.F., De Resende, M.A. & Sluka, K.A.
924 Transcutaneous electrical nerve stimulation at both high and low frequencies
925 activates ventrolateral periaqueductal grey to decrease mechanical hyperalgesia
926 in arthritic rats. *Neuroscience* **163**, 1233-1241 (2009).
927 19. Leonard, G., Goffaux, P. & Marchand, S. Deciphering the role of endogenous
928 opioids in high-frequency TENS using low and high doses of naloxone. *Pain*
929 **151**, 215-219 (2010).
930 20. de Resende, M.A., Silva, L.F., Sato, K., Arendt-Nielsen, L. & Sluka, K.A.
931 Blockade of opioid receptors in the medullary reticularis nucleus dorsalis, but
932 not the rostral ventromedial medulla, prevents analgesia produced by diffuse
933 noxious inhibitory control in rats with muscle inflammation. *J Pain* **12**, 687-697
934 (2011).
935 21. Maeda, Y., Lisi, T.L., Vance, C.G. & Sluka, K.A. Release of GABA and
936 activation of GABA(A) in the spinal cord mediates the effects of TENS in rats.
937 *Brain Res* **1136**, 43-50 (2007).
938 22. Sluka, K.A., Deacon, M., Stibal, A., Strissel, S. & Terpstra, A. Spinal blockade
939 of opioid receptors prevents the analgesia produced by TENS in arthritic rats. *J*
940 *Pharmacol Exp Ther* **289**, 840-846 (1999).
941 23. Melzack, R. & Wall, P.D. Pain mechanisms: a new theory. *Science* **150**, 971-
942 979 (1965).
943 24. Fried, T., Johnson, R. & McCracken, W. Transcutaneous electrical nerve
944 stimulation: its role in the control of chronic pain. *Arch Phys Med Rehabil* **65**,
945 228-231 (1984).
946 25. Garrison, D.W. & Foreman, R.D. Decreased activity of spontaneous and
947 noxiously evoked dorsal horn cells during transcutaneous electrical nerve
948 stimulation (TENS). *Pain* **58**, 309-315 (1994).
949 26. Choi, J.C.*, et al.* Brain mechanisms of pain relief by transcutaneous electrical
950 nerve stimulation: A functional magnetic resonance imaging study. *Eur J Pain*
951 **20**, 92-105 (2016).
952 27. Kara, M.*, et al.* Quantification of the effects of transcutaneous electrical nerve
953 stimulation with functional magnetic resonance imaging: a double-blind
954 randomized placebo-controlled study. *Arch Phys Med Rehabil* **91**, 1160-1165

(2010).

28. Yarnitsky, D. Role of endogenous pain modulation in chronic pain mechanisms and treatment. *Pain* **156 Suppl 1**, S24-S31 (2015).

29. Faghani Jadidi, A., Stevenson, A.J.T., Zarei, A.A., Jensen, W. & Lontis, R. Effect of Modulated TENS on Corticospinal Excitability in Healthy Subjects. *Neuroscience* **485**, 53-64 (2022).

30. Cohen-Adad, J.*, et al.* BOLD signal responses to controlled hypercapnia in human spinal cord. *Neuroimage* **50**, 1074-1084 (2010).

31. Finsterbusch, J., Sprenger, C. & Buchel, C. Combined T2*-weighted measurements of the human brain and cervical spinal cord with a dynamic shim update. *Neuroimage* **79**, 153-161 (2013).

32. Islam, H., Law, C.S.W., Weber, K.A., Mackey, S.C. & Glover, G.H. Dynamic per slice shimming for simultaneous brain and spinal cord fMRI. *Magn Reson Med* **81**, 825-838 (2019).

33. Fields, H.L., & Basbaum, A.I. Central nervous system mechanisms of pain modulation. in *Textbook of pain* (ed. P. D. Wall, R.M.) 243-257 (Chruchill Livingston, New York, 1994).

34. Tinnermann, A., Geuter, S., Sprenger, C., Finsterbusch, J. & Buchel, C. Interactions between brain and spinal cord mediate value effects in nocebo hyperalgesia. *Science* **358**, 105-108 (2017).

35. Tinnermann, A., Sprenger, C. & Buchel, C. Opioid analgesia alters corticospinal coupling along the descending pain system in healthy participants. *Elife* **11**, e74293 (2022).

36. Oliva, V., Hartley-Davies, R., Moran, R., Pickering, A.E. & Brooks, J.C. Simultaneous brain, brainstem, and spinal cord pharmacological-fMRI reveals involvement of an endogenous opioid network in attentional analgesia. *Elife* **11**, e71877 (2022).

37. Felten, D.L., O'Banion, M.K. & Maida, M.E. *Netter's atlas of neuroscience*, (Elsevier Health Sciences, 2015).

38. Jensen, M.P., Karoly, P. & Braver, S. The measurement of clinical pain intensity: a comparison of six methods. *Pain* **27**, 117-126 (1986).

39. Price, D.D. Psychological and neural mechanisms of the affective dimension of pain. *Science* **288**, 1769-1772 (2000).

40. Brooks, J.C., *et al.* Stimulus site and modality dependence of functional activity within the human spinal cord. *Journal of Neuroscience* **32**, 6231-6239 (2012).
41. Brooks, J.C., Nurmikko, T.J., Bimson, W.E., Singh, K.D. & Roberts, N. fMRI of thermal pain: effects of stimulus laterality and attention. *Neuroimage* **15**, 293-301 (2002).
42. Zarei, A.A., Jensen, W., Faghani Jadidi, A., Lontis, E.R. & Atashzar, S.F. Gamma-band enhancement of functional brain connectivity following transcutaneous electrical nerve stimulation. *J Neural Eng* **19**, 026020 (2022).
43. Le Bars, D., Dickenson, A.H. & Besson, J.M. Diffuse noxious inhibitory controls (DNIC). I. Effects on dorsal horn convergent neurones in the rat. *Pain* **6**, 283-304 (1979).
44. Ossipov, M.H., Dussor, G.O. & Porreca, F. Central modulation of pain. *The Journal of clinical investigation* **120**, 3779-3787 (2010).
45. DeSantana, J.M., da Silva, L.F.S. & Sluka, K.A. Cholecystokinin receptors mediate tolerance to the analgesic effect of TENS in arthritic rats. *Pain* **148**, 84-93 (2010).
46. Radhakrishnan, R., *et al.* Spinal 5-HT2 and 5-HT3 receptors mediate low, but not high, frequency TENS-induced antihyperalgesia in rats. *Pain* **105**, 205-213 (2003).
47. Geuter, S., *et al.* Multiple Brain Networks Mediating Stimulus-Pain Relationships in Humans. *Cereb Cortex* **30**, 4204-4219 (2020).
48. Kalra, A., Urban, M.O. & Sluka, K.A. Blockade of opioid receptors in rostral ventral medulla prevents antihyperalgesia produced by transcutaneous electrical nerve stimulation (TENS). *J Pharmacol Exp Ther* **298**, 257-263 (2001).
49. Resende, M.A.D., Silva, L.F.S., Sato, K., Arendt-Nielsen, L. & Sluka, K.A. Blockade of Opioid Receptors in the Medullary Reticularis Nucleus Dorsalis, but not the Rostral Ventromedial Medulla, Prevents Analgesia Produced by Diffuse Noxious Inhibitory Control in Rats With Muscle Inflammation. *Journal of Pain* **12**, 687-697 (2011).
50. Ojala, K.E., Chu, Y., Finsterbusch, J. & Büchel, C. Conditioned pain modulation of pressure pain is associated with reduced activation in the parietal operculum and posterior insula. *bioRxiv*, 2023.2008. 2023.554467 (2023).
51. Ploner, M., Schmitz, F., Freund, H.J. & Schnitzler, A. Parallel activation of

primary and secondary somatosensory cortices in human pain processing. *J Neurophysiol* **81**, 3100-3104 (1999).

52. Chen, T.L.*, et al.* Human secondary somatosensory cortex is involved in the processing of somatosensory rare stimuli: an fMRI study. *Neuroimage* **40**, 1765-1771 (2008).

53. Rossi-Pool, R., Zainos, A., Alvarez, M., Diaz-deLeon, G. & Romo, R. A continuum of invariant sensory and behavioral-context perceptual coding in secondary somatosensory cortex. *Nat Commun* **12**, 2000 (2021).

54. Condylis, C.*, et al.* Context-Dependent Sensory Processing across Primary and Secondary Somatosensory Cortex. *Neuron* **106**, 515-525 e515 (2020).

55. Ferezou, I., Haiss, F., Gentet, L.J., Aronoff, R., Weber, B. & Petersen, C.C. Spatiotemporal dynamics of cortical sensorimotor integration in behaving mice. *Neuron* **56**, 907-923 (2007).

56. Pala, A. & Stanley, G.B. Ipsilateral Stimulus Encoding in Primary and Secondary Somatosensory Cortex of Awake Mice. *J Neurosci* **42**, 2701-2715 (2022).

57. Ploner, M., Gross, J., Timmermann, L. & Schnitzler, A. Cortical representation of first and second pain sensation in humans. *Proceedings of the National Academy of Sciences* **99**, 12444-12448 (2002).

58. Tracey, I. & Mantyh, P.W. The cerebral signature for pain perception and its modulation. *Neuron* **55**, 377-391 (2007).

59. Gao, K., Kim, Y.H. & Mason, P. SEROTONERGIC pontomedullary neurons are not activated by antinociceptive stimulation in the periaqueductal gray. *J Neurosci* **17**, 3285-3292 (1997).

60. Buchel, C., Geuter, S., Sprenger, C. & Eippert, F. Placebo analgesia: a predictive coding perspective. *Neuron* **81**, 1223-1239 (2014).

61. Crawford, L.S.*, et al.* Brainstem Mechanisms of Pain Modulation: A within-Subjects 7T fMRI Study of Placebo Analgesic and Nocebo Hyperalgesic Responses. *J Neurosci* **41**, 9794-9806 (2021).

62. Brooks, J.C., Davies, W.E. & Pickering, A.E. Resolving the Brainstem Contributions to Attentional Analgesia. *J Neurosci* **37**, 2279-2291 (2017).

63. Eippert, F. & Tracey, I. Pain and the PAG: learning from painful mistakes. *Nat Neurosci* **17**, 1438-1439 (2014).

1054 64. Waters, A. & Lumb, B. Inhibitory effects evoked from both the lateral and
1055 ventrolateral periaqueductal grey are selective for the nociceptive responses of
1056 rat dorsal horn neurones. *Brain research* **752**, 239-249 (1997).
1057 65. Bandler, R. & Shipley, M.T. Columnar organization in the midbrain
1058 periaqueductal gray: modules for emotional expression? *Trends Neurosci* **17**,
1059 379-389 (1994).
1060 66. Coulombe, M.A., Erpelding, N., Kucyi, A. & Davis, K.D. Intrinsic functional
1061 connectivity of periaqueductal gray subregions in humans. *Hum Brain Mapp* **37**,
1062 1514-1530 (2016).
1063 67. Sims-Williams, H.*, et al.* Deep brain stimulation of the periaqueductal gray
1064 releases endogenous opioids in humans. *Neuroimage* **146**, 833-842 (2017).
1065 68. Kucyi, A. & Davis, K.D. The Neural Code for Pain: From Single-Cell
1066 Electrophysiology to the Dynamic Pain Connectome. *Neuroscientist* **23**, 397-
1067 414 (2017).
1068 69. Bingel, U., Lorenz, J., Schoell, E., Weiller, C. & Buchel, C. Mechanisms of
1069 placebo analgesia: rACC recruitment of a subcortical antinociceptive network.
1070 *Pain* **120**, 8-15 (2006).
1071 70. Eippert, F.*, et al.* Activation of the opioidergic descending pain control system
1072 underlies placebo analgesia. *Neuron* **63**, 533-543 (2009).
1073 71. Floyd, N.S., Price, J.L., Ferry, A.T., Keay, K.A. & Bandler, R. Orbitomedial
1074 prefrontal cortical projections to distinct longitudinal columns of the
1075 periaqueductal gray in the rat. *J Comp Neurol* **422**, 556-578 (2000).
1076 72. An, X., Bandler, R., Ongur, D. & Price, J.L. Prefrontal cortical projections to
1077 longitudinal columns in the midbrain periaqueductal gray in macaque monkeys.
1078 *J Comp Neurol* **401**, 455-479 (1998).
1079 73. Bushnell, M.C., Ceko, M. & Low, L.A. Cognitive and emotional control of pain
1080 and its disruption in chronic pain. *Nat Rev Neurosci* **14**, 502-511 (2013).
1081 74. Villemure, C. & Bushnell, M.C. Mood influences supraspinal pain processing
1082 separately from attention. *J Neurosci* **29**, 705-715 (2009).
1083 75. Linnman, C., Moulton, E.A., Barmettler, G., Becerra, L. & Borsook, D.
1084 Neuroimaging of the periaqueductal gray: state of the field. *Neuroimage* **60**,
1085 505-522 (2012).
1086 76. Wang, L.H., Ding, W.Q. & Sun, Y.G. Spinal ascending pathways for

somatosensory information processing. *Trends Neurosci* **45**, 594-607 (2022).

77. Sprenger, C., Finsterbusch, J. & Buchel, C. Spinal cord-midbrain functional connectivity is related to perceived pain intensity: a combined spino-cortical FMRI study. *J Neurosci* **35**, 4248-4257 (2015).

78. Bressler, S.L. & Menon, V. Large-scale brain networks in cognition: emerging methods and principles. *Trends Cogn Sci* **14**, 277-290 (2010).

79. Chesterton, L.S., Foster, N.E., Wright, C.C., Baxter, G.D. & Barlas, P. Effects of TENS frequency, intensity and stimulation site parameter manipulation on pressure pain thresholds in healthy human subjects. *Pain* **106**, 73-80 (2003).

80. Bi, J. & Ennis, D.M. Sensory Thresholds: Concepts and Methods. *Journal of Sensory Studies* **13**, 133-148 (2007).

81. Ruscheweyh, R., Marziniak, M., Stumpenhorst, F., Reinholz, J. & Knecht, S. Pain sensitivity can be assessed by self-rating: development and validation of the Pain Sensitivity Questionnaire. *Pain* **146**, 65-74 (2009).

82. McCracken, L.M., Zayfert, C. & Gross, R.T. The Pain Anxiety Symptoms Scale: development and validation of a scale to measure fear of pain. *Pain* **50**, 67-73 (1992).

83. Sullivan, M.J., Bishop, S.R. & Pivik, J. The pain catastrophizing scale: development and validation. *Psychological assessment* **7**, 524 (1995).

84. Roelofs, J., Peters, M.L., McCracken, L. & Vlaeyen, J.W. The pain vigilance and awareness questionnaire (PVAQ): further psychometric evaluation in fibromyalgia and other chronic pain syndromes. *Pain* **101**, 299-306 (2003).

85. Spielberger, C.D., Gonzalez-Reigosa, F., Martinez-Urrutia, A., Natalicio, L.F. & Natalicio, D.S. The state-trait anxiety inventory. *Revista Interamericana de Psicologia/Interamerican journal of psychology* **5**(1971).

86. Beck, A.T., Steer, R.A. & Carbin, M.G. Psychometric properties of the Beck Depression Inventory: Twenty-five years of evaluation. *Clinical psychology review* **8**, 77-100 (1988).

87. Davis, M.H. Interpersonal reactivity index. (1980).

88. Behroozi, M. & Daliri, M.R. Software tools for the analysis of functional magnetic resonance imaging. *Basic and Clinical Neuroscience* **3**, 71-83 (2012).

89. McNeil, D.W. & Rainwater, A.J., 3rd. Development of the Fear of Pain Questionnaire--III. *J Behav Med* **21**, 389-410 (1998).

90. Rolke, R., *et al.* Quantitative sensory testing: a comprehensive protocol for clinical trials. *Eur J Pain* **10**, 77-88 (2006).
91. Todd, N., Moeller, S., Auerbach, E.J., Yacoub, E., Flandin, G. & Weiskopf, N. Evaluation of 2D multiband EPI imaging for high-resolution, whole-brain, task-based fMRI studies at 3T: Sensitivity and slice leakage artifacts. *Neuroimage* **124**, 32-42 (2016).
92. Mugler III, J.P. & Brookeman, J.R. Three-dimensional magnetization-prepared rapid gradient-echo imaging (3D MP RAGE). *Magnetic resonance in medicine* **15**, 152-157 (1990).
93. Jenkinson, M., Beckmann, C.F., Behrens, T.E., Woolrich, M.W. & Smith, S.M. Fsl. *Neuroimage* **62**, 782-790 (2012).
94. De Leener, B., *et al.* SCT: Spinal Cord Toolbox, an open-source software for processing spinal cord MRI data. *Neuroimage* **145**, 24-43 (2017).
95. Smith, S.M., *et al.* Accurate, robust, and automated longitudinal and cross-sectional brain change analysis. *Neuroimage* **17**, 479-489 (2002).
96. De Leener, B., Fonov, V.S., Collins, D.L., Callot, V., Stikov, N. & Cohen-Adad, J. PAM50: Unbiased multimodal template of the brainstem and spinal cord aligned with the ICBM152 space. *Neuroimage* **165**, 170-179 (2018).
97. Brooks, J.C., *et al.* Physiological noise modelling for spinal functional magnetic resonance imaging studies. *Neuroimage* **39**, 680-692 (2008).
98. Kong, Y., Jenkinson, M., Andersson, J., Tracey, I. & Brooks, J.C. Assessment of physiological noise modelling methods for functional imaging of the spinal cord. *Neuroimage* **60**, 1538-1549 (2012).
99. Eippert, F., Kong, Y., Jenkinson, M., Tracey, I. & Brooks, J.C.W. Denoising spinal cord fMRI data: Approaches to acquisition and analysis. *Neuroimage* **154**, 255-266 (2017).
100. Saritas, E.U., Holdsworth, S.J. & Bammer, R. Susceptibility Artifacts. in *Quantitative MRI of the Spinal Cord* (eds. Cohen-Adad, J. & Wheeler-Kingshott, C.A.M.) 91-105 (Academic Press, San Diego, 2014).
101. Smith, S.M., *et al.* Advances in functional and structural MR image analysis and implementation as FSL. *Neuroimage* **23**, S208-S219 (2004).
102. Jezzard, P. & Balaban, R.S. Correction for geometric distortion in echo planar images from B0 field variations. *Magn Reson Med* **34**, 65-73 (1995).

103. Henson, R., Buechel, C., Josephs, O. & Friston, K. The slice-timing problem in event-related fMRI. *NeuroImage* **9**, 125- (1999).

104. Jenkinson, M., Bannister, P., Brady, M. & Smith, S. Improved optimization for the robust and accurate linear registration and motion correction of brain images. *Neuroimage* **17**, 825-841 (2002).

105. Andersson, J.L., Jenkinson, M. & Smith, S. Non-linear registration, aka Spatial normalisation FMRIB technical report TR07JA2. *FMRIB Analysis Group of the University of Oxford* **2**, e21 (2007).

106. Woolrich, M.W., Ripley, B.D., Brady, M. & Smith, S.M. Temporal autocorrelation in univariate linear modeling of FMRI data. *Neuroimage* **14**, 1370-1386 (2001).

107. Beckmann, C.F., Jenkinson, M. & Smith, S.M. General multilevel linear modeling for group analysis in FMRI. *Neuroimage* **20**, 1052-1063 (2003).

108. Woolrich, M.W., Behrens, T.E., Beckmann, C.F., Jenkinson, M. & Smith, S.M. Multilevel linear modelling for FMRI group analysis using Bayesian inference. *Neuroimage* **21**, 1732-1747 (2004).

109. Brooks, J.C., Faull, O.K., Pattinson, K.T. & Jenkinson, M. Physiological noise in brainstem FMRI. *Front Hum Neurosci* **7**, 623 (2013).

110. Worsley, K.J., Evans, A.C., Marrett, S. & Neelin, P. A three-dimensional statistical analysis for CBF activation studies in human brain. *J Cereb Blood Flow Metab* **12**, 900-918 (1992).

111. Nichols, T.E. & Holmes, A.P. Nonparametric permutation tests for functional neuroimaging: a primer with examples. *Hum Brain Mapp* **15**, 1-25 (2002).

112. Desikan, R.S.*, et al.* An automated labeling system for subdividing the human cerebral cortex on MRI scans into gyral based regions of interest. *Neuroimage* **31**, 968-980 (2006).

113. Smith, S.M. & Nichols, T.E. Threshold-free cluster enhancement: addressing problems of smoothing, threshold dependence and localisation in cluster inference. *Neuroimage* **44**, 83-98 (2009).

114. Winkler, A.M., Ridgway, G.R., Webster, M.A., Smith, S.M. & Nichols, T.E. Permutation inference for the general linear model. *Neuroimage* **92**, 381-397 (2014).

115. Treede, R.D., Kenshalo, D.R., Gracely, R.H. & Jones, A.K. The cortical

representation of pain. *Pain* **79**, 105-111 (1999).